1 **Representation of a two-way coupled irrigation system in the Common Land Model**

2 Shulei Zhang[1,#], Hongbin Liang[1,#], Fang Li[2], Xingjie Lu[1], Yongjiu Dai[1]

3 *[1] Southern Marine Science and Engineering Guangdong Laboratory (Zhuhai), School of*
4 *Atmospheric Sciences, Sun Yat-sen University, Guangzhou, China*
5 *[2]International Center for Climate and Environment Sciences, Institute of Atmospheric Physics,*
6 *Chinese Academy of Sciences, Beijing, 100029, China*
7 *Corresponding Author: Shulei Zhang (zhangshlei@mail.sysu.edu.cn) & Hongbin Liang*
8 *(lianghb25@mail2.sysu.edu.cn)*
9 *[#] These authors contributed equally to this work.*

10

11 **Abstract**

12 Human land–water management, especially irrigation water withdrawal and use, significantly
13 impacts the global and regional water cycle, energy budget, and near-surface climate. While land
14 surface models are widely used to explore and predict the impacts of irrigation, the irrigation
15 system representation in these models is still in its early stages. This study enhances the
16 Common Land Model (CoLM) by introducing a two-way coupled irrigation module. This
17 module includes an irrigation water demand scheme based on soil moisture deficit, an irrigation
18 application scheme considering four major irrigation methods, and an irrigation water
19 withdrawal scheme that incorporates multiple water source constraints by integrating CoLM with
20 a river routing model and a reservoir operation scheme. Crucially, it explicitly accounts for the
21 feedback between irrigation water demand and supply, which is constrained by available surface
22 water (i.e., runoff, streamflow, reservoir storage) and groundwater. Simulations conducted from
23 2001 to 2016 at a 0.25° spatial resolution across the contiguous United States reveal that the
24 model effectively reproduces irrigation withdrawals, their spatial distribution, and water source
25 proportions, aligning well with reported state-level statistics. Comprehensive validation
26 demonstrates that the new module significantly improves model accuracy in simulating regional
27 energy dynamics (sensible heat, latent heat, and surface temperature), hydrology (river flow),
28 and agricultural outputs (yields for maize, soybean, and wheat). Application analyses highlight
29 the potential of the enhanced CoLM as a valuable tool for predicting irrigation-driven climate
30 impacts and assessing water use and scarcity. This research offers a pathway for a more holistic
31 representation of fluxes in irrigated areas and human-water interactions within land surface
32 models. It is valuable for exploring the interconnected evolution of climate, water resources,
33 agricultural production, and irrigation activities, while supporting sustainable water management
34 decisions in a changing climate.

## 1. Introduction

Freshwater resources are indispensable for human society. Since 1900, the global population has increased more than fourfold, leading to a nearly sixfold rise in water withdrawals, from approximately 500 km³ per year in 1900 to about 3000 km³ per year in 2000, with agriculture being the dominant water user (Pokhrel et al., 2016). Around 70% of global freshwater has been withdrawn for irrigation (Campbell et al., 2017), accounting for 90% of consumptive water use (Siebert and Döll, 2010), with irrigated areas providing approximately 40% of global food production on just 2.5% of global land (Abdullah, 2006). Accompanied by significant socioeconomic benefits, these intense human land-water management practices have profoundly altered Earth's surface and impacted terrestrial water and energy cycles (Ketchum et al., 2023; Nocco et al., 2019; Rappin et al., 2022; Thiery et al., 2017; de Vrese et al., 2016). The demand for irrigation water is anticipated to rise with the growing global population and food demand, while climate-warming-induced droughts are likely to exacerbate this need (McDermid et al., 2023; Mehta et al., 2024; Yang et al., 2023). Therefore, understanding and quantifying the impacts of irrigation water management in human-Earth system interactions are crucial for developing strategies to sustainably manage these resources amidst changing climatic and demographic conditions.

Irrigation practices transfer water from various sources, such as rivers, lakes, reservoirs, and aquifers, into agricultural systems, directly affecting the magnitude and timing of runoff and river flow (Ketchum et al., 2023). The rising irrigation demand has spurred increased construction of reservoirs and diversions, resulting in both local and downstream impacts. In some regions, water extraction for irrigation has reduced the availability of both surface and groundwater (Döll et al., 2014). Besides modifying water fluxes, irrigation also influences regional climates both locally and remotely. Locally, it alters surface albedo, evapotranspiration, and surface soil moisture, impacting regional radiation and energy balances and affecting temperature, humidity, and precipitation through land-atmosphere feedback (Chen and Dirmeyer, 2019; Kang and Eltahir, 2018; Li et al., 2022; McDermid et al., 2017; Nocco et al., 2019). Remotely, it affects climate through complex interactions between altered temperature and moisture gradients and larger-scale processes such as atmospheric circulation and wave activity (Douglas et al., 2009; Phillips et al., 2022; de Vrese et al., 2016).

Earth system models (ESMs) are powerful tools for examining the interactions and feedback among the intricately intertwined processes of the Earth system, both in the past and future. Land surface models (LSMs) are a crucial component of ESMs. Due to the complex dynamics of natural hydrological processes and anthropogenic activities, describing human-water interactions has been recognized as a significant challenge in Land surface modeling (Nazemi and Wheater, 2015). In recent years, targeted efforts have aimed to address this deficiency, yet water use remains largely underrepresented or in a nascent stage within LSMs (Blyth et al., 2021; Taranu et al., 2024). Meanwhile, global hydrological models (GHMs), originally designed for water

73   resource assessment, have undergone continuous improvements over the last three decades to
74   explicitly represent human water use (Hanasaki et al., 2018; Liang et al., 1994; Müller Schmied
75   et al., 2021; Sood and Smakhtin, 2015; Sutanudjaja et al., 2018; Tang et al., 2007). These models
76   enable the determination of the spatial distribution and temporal evolution of water resources and
77   water stress for both humans and other biota under the pressures of global change (Döll et al.,
78   2018; Schewe et al., 2014; Schlosser et al., 2014). These advancements have offered valuable
79   insights for incorporating human water use into LSMs.

80   Parameterizing irrigation water use and modeling its impacts in GHMs and LSMs has been
81   approached using different assumptions and simplifications in three key aspects: irrigation
82   demands, irrigation methods, and irrigation water supplies/withdrawals. The first aspect is
83   estimating irrigation water demands. Models estimate these demands using either a root-zone
84   soil moisture deficit approach or a crop-specific potential evapotranspiration approach. The root-
85   zone soil moisture deficit approach estimates irrigation demand as the water needed to keep root-
86   zone soil moisture (usually within the top meter of soil) above a certain threshold during the
87   growing season (normally a certain percentage of field capacity or soil saturation) (Ozdogan et
88   al., 2010). The crop-specific potential evapotranspiration approach estimates irrigation needs
89   based on the difference between crop-specific potential evapotranspiration and simulated
90   unirrigated evapotranspiration, or between potential and effective precipitation under well-
91   watered conditions where crops transpire at their maximum rate (Müller Schmied et al., 2021).
92   Notably, LSMs generally do not use potential evapotranspiration to estimate irrigation demand.

93   The second aspect concerns the representation of irrigation methods. Many models simplify
94   irrigation application by directly modifying soil moisture or treating it as additional rainfall
95   across all irrigated land, overlooking the diversity of irrigation techniques employed in various
96   parts of the world or by different farmers (Li et al., 2024a; Lu et al., 2015; de Vrese et al., 2018).
97   Recently, some models have started integrating specific irrigation techniques for certain crops or
98   regions. For instance, LPJmL includes sprinkler, drip, and surface irrigation methods, and CLM
99   incorporates drip, sprinkler, flood, and paddy irrigation methods (Jägermeyr et al., 2015; Yao et
100  al., 2022). Different irrigation techniques affect farmland hydrological processes and irrigation
101  efficiency in distinct ways. For example, drip and surface irrigation methods avoid interception
102  losses observed with sprinkler (Nair et al., 2013).

103  Third is the representation of irrigation water supplies/withdrawals, which is particularly critical
104  as it involves the interaction between multiple processes or modules, such as hydrological and
105  agricultural systems. However, explicit representation of these interactions remains largely
106  absent in LSMs, despite the extensive modeling experience provided by GHMs. Such modeling
107  first requires identifying the sources of irrigation water, typically categorized into surface water
108  and groundwater. Surface water sources are normally constrained by available runoff,
109  streamflow, and storage such as lakes and reservoirs. Accessing these sources, such as rivers and
110  reservoirs, necessitates coupling with river routing and reservoir modules, which are well-

111   represented in many GHMs (Biemans et al., 2011; Hanasaki et al., 2018). Groundwater is
112   typically divided into renewable sources (baseflow or dynamic groundwater levels) and
113   nonrenewable sources (fossil groundwater). Some models assume an inexhaustible supply of
114   nonrenewable groundwater to meet irrigation demands, neglecting irrigation shortages caused by
115   water scarcity (Zhou et al., 2020). Additionally, some GHMs incorporate alternative sources,
116   such as inter-regional water transfers and seawater desalination (Hanasaki et al., 2018;
117   Sutanudjaja et al., 2018). A second critical aspect of irrigation water supply modeling is
118   determining the allocation of irrigation water among different sources, including the
119   prioritization of water usage. Various models adopt different assumptions for this allocation. For
120   example, H08 prioritizes surface water (Hanasaki et al., 2018), while WBMplus prioritizes
121   reservoirs and groundwater (Wisser et al., 2010). PCR-GLOBWB uses an empirical approach
122   that allocates groundwater use based on comparisons between baseflow conditions and long-term
123   historical climatology, capturing feedback between water supply and demand (Sutanudjaja et al.,
124   2018). Another common approach is to assume a predefined allocation ratio based on water
125   withdrawal infrastructure (e.g., Siebert et al., 2010), using this ratio to divide total irrigation
126   abstractions between groundwater and surface water (Arboleda-Obando et al., 2024; Leng et al.,
127   2015). Despite these advances, the representation of water extraction and the coupling of
128   irrigation and hydrological systems in LSMs is still in its early stages. Most irrigation-enabled
129   models still assume an unlimited water supply, failing to account for constraints imposed by
130   water availability (Druel et al., 2022; Yao et al., 2022; Zhou et al., 2020).

131   The Common Land Model (CoLM; Dai et al., 2003), derived from the Community Land Model
132   (CLM), is a widely used land surface model that integrates ecological, hydrological, and
133   biophysical processes. In recent years, it has further incorporated various physical processes such
134   as lakes, wetlands, and dynamic vegetation, enhancing the representation of energy and water
135   exchanges among soil, vegetation, snow, and atmosphere. CoLM has been successfully
136   implemented in global atmospheric models, such as GRAPES, CWRF, and CAS-ESM2.0 (Shen
137   et al., 2021; Yuan and Liang, 2011; Zhang et al., 2020a). Despite significant advancements in
138   parameterizing natural land surface processes, the representation of human activities in CoLM
139   remains at an early stage. Recently, CoLM has further integrated a crop module, providing a
140   foundation for considering irrigation and its interactions with natural water systems.

141   To enhance the representation of human–water interactions in land surface models, we introduce
142   a new irrigation module for CoLM. This module provides a comprehensive framework for
143   simulating the entire irrigation water system, including water demand, withdrawal, and
144   utilization. It incorporates an irrigation water demand scheme based on soil moisture deficits, an
145   irrigation application scheme accounting for four major irrigation methods, and an irrigation
146   water withdrawal scheme that incorporates multiple water source constraints by integrating
147   CoLM with a river routing model and a reservoir operation scheme. A key focus of this module
148   is the bidirectional coupling between irrigation water demand and supply, alongside a detailed
149   representation of water withdrawals from different sources. Section 2 provides a detailed

4

150 description of the module and its implementation, including an overview of CoLM, the datasets
151 used for simulation and validation, and the experimental design. Section 3 validates the module's
152 performance in simulating irrigation water withdrawals using reported data and compares its
153 results to other hydrological models. It also assesses improvements in model accuracy for
154 regional energy dynamics (sensible heat, latent heat, and surface temperature), hydrology (river
155 flow), and agricultural outputs (maize, soybean, and wheat yields). Section 4 demonstrates two
156 key applications of the module: analyzing irrigation impacts on the energy budget and evaluating
157 irrigation water security. Finally, we discuss the module's current limitations and propose
158 potential future improvements.

## 2. Materials and Methods

### 2.1 Description of CoLM and its crop module

161 The Common Land Model (CoLM) is one of the most advanced land surface models widely used
162 to simulate the Water–Energy–Carbon Nexus. The original version of CoLM (Dai et al., 2003)
163 combines the three land surface models: the Land Surface Model (LSM; Bonan, 1996), the
164 Biosphere-Atmosphere Transfer Scheme (BATS; Dickinson et al., 1993), and the 1994 version of
165 the Chinese Academy of Sciences Institute of Atmospheric Physics LSM (IAP94; Dai and Zeng,
166 1997). CoLM2014 integrates the Catchment-Based Macro-Scale Floodplain model (CaMa-
167 Flood; Yamazaki et al., 2011), enabling river routing calculations within the model. Specifically,
168 runoff generated by CoLM is transferred to CaMa-Flood for routing through the river network.
169 CaMa-Flood represents the river network as a series of irregular unit catchments, defined
170 through sub-grid topographic parameters. River discharge and other flow characteristics are
171 computed using the local inertial equations along the river network, allowing for detailed flow
172 dynamics across catchments.

173 In CoLM2024, the 'patch' serves as the fundamental computational unit to account for land
174 surface heterogeneity (Figure S1). Based on land type, patches are divided into five types:
175 vegetation (including bare soil), urban, wetlands, glaciers, and water bodies. The vegetation
176 patch is further classified into natural vegetation and crops, represented using the Plant
177 Functional Type (PFT) approach. Under this framework, all natural vegetation within a grid cell
178 is treated as a single patch, sharing common soil thermal and moisture conditions while radiative
179 and photosynthesis processes are simulated independently. When the crop model is activated,
180 each crop type (distinguishing between rainfed and irrigated crops) is treated as an independent
181 patch. This means that the calculations of soil moisture and thermal processes for each crop
182 patch remain independent, without shared water and heat dynamics.

183 At each patch, the primary thermal processes include precipitation phase change, radiation
184 transfer, temperature calculations for leaves, snow, and soil, turbulent exchange, etc. The key
185 hydrological processes include canopy interception, evapotranspiration, surface runoff,

infiltration, soil water vertical movement, subsurface runoff, groundwater, river routing, etc. Specifically, the two-big-leaf scheme is employed to compute radiation transfer, leaf temperature, photosynthesis and transpiration (Dai et al., 2004; Yuan et al., 2017). Surface turbulent exchange is simulated using similarity theory (Liu et al., 2022; Zeng and Dickinson, 1998). Soil and snow temperature are determined using the heat diffusion equation, considering only vertical exchange (Dai and Yuan, 2014). Canopy interception is calculated same as CoLM2014 with considering the leaf angle and precipitation phase (Dai and Yuan, 2014; Sellers et al., 1996). Soil water vertical movement is simulated by the Richards equation and Buckingham-Darcy's law with using the Campbell soil water characteristic curve scheme to close the Richards equation (Buckingham, 1907; Campbell, 1974; Richards, 1931). Surface and subsurface runoff are estimated using the SIMTOP approach (Niu et al., 2005). When the irrigation scheme is activated, irrigation water is applied to the canopy or top soil according to predefined irrigation methods and simulated irrigation amounts, thereby influencing the soil moisture and thermal processes within the irrigated patches.

The CoLM2024 version incorporates substantial updates over CoLM2014, particularly by introducing representations of biogeochemical cycles and human activity processes (e.g., crop growth and reservoir management). The new crop module introduces a phenological development scheme based on accumulated temperature, a biomass allocation scheme among different plant organs, and fertilization schemes (Drewniak et al., 2013). Crops are categorized into four organ pools: leaves, stems, fine roots, and grains. The growth stages are divided into three phases: sowing to emergence, emergence to grain filling, and grain filling to maturity, with carbon allocation ratios to roots, stems, leaves, and grains varying across these phases. Upon maturation, crops are harvested, with part of the carbon from the grains contributing to the yield, while a small portion (3g) is reserved as seeds for the next growing season. For carbon assimilation, the module employs Farquhar's photosynthesis scheme (Collatz et al., 1992; Farquhar et al., 1980) and Ball-Berry's stomatal model (Ball et al., 1987; Collatz et al., 1991), treating maize as a C4 crop and other crops as C3. Additionally, the module accounts for the effects of heat stress, water stress, nitrogen stress, and ozone stress on yield (Li et al., 2024b; Lombardozzi et al., 2020). The module has been calibrated for various crops, including maize, soybean, spring and winter wheat, rice, cotton, and sugarcane, enabling accurate simulation of crop yields.

**2.2 Two-way coupled irrigation water use module**

**2.2.1 Irrigation demand**

The irrigation demand is calculated using the soil moisture deficit method (Leng et al., 2017; Ozdogan et al., 2010; Yao et al., 2022). During the crop growth stage, irrigation is triggered at 6 a.m. local time if the soil moisture in the root zone ($z_{irrig}$=1m) falls below the threshold value ($\omega_{thresh}$). The total irrigation water demand ($D_{irrig}$, mm) is then calculated using Equation (1):

$$223 \qquad D_{\text{irrig}} = \begin{cases} \omega_{\text{irrig}} - \omega_{\text{avail}} & \omega_{\text{avail}} \leqslant \omega_{\text{thresh}} \\ 0 & \omega_{\text{avail}} > \omega_{\text{thresh}} \end{cases} \qquad (1)$$

224    where $\omega_{\text{avail}}$ is the total soil water amount in the root zone (mm); $\omega_{\text{irrig}}$ is the irrigation target

225    threshold (mm), calculated using Equation (2):

$$226 \qquad \omega_{\text{irrig}} = f_{\text{irrig}}(\omega_{\text{target}} - \omega_{\text{wilt}}) + \omega_{\text{wilt}} \qquad (2)$$

227    where $\omega_{\text{wilt}}$ is the wilting point soil water amount in the root zone (mm), calculated as the sum of

228    soil water at the wilting point for each soil layer ($\sum_{j=1}^{N_{\text{irr}}} \theta_{\text{wilt}} \Delta z_j$); $\omega_{target}$ is the target soil water

229    amount in the root zone (mm), calculated as the sum of target soil water for each soil layer

230    ($\sum_{j=1}^{N_{\text{irr}}} \theta_{\text{target}} \Delta z_j$). $N_{\text{irr}}$ is the number of soil layers in the root zone and $\Delta z_j$ is the thickness of each

231    soil layer (m). The target ($\theta_{\text{target}}$) and wilting point ($\theta_{\text{wilt}}$) soil moisture ($m^3/m^3$) for each layer are

232    calculated based on the corresponding soil water potential ($\Phi_{\text{target}}$ and $\Phi_{\text{wilt}}$). $f_{\text{irrig}}$ is a weighting

233    coefficient ranging from 0 to 1, controlling the extent to which soil water amount approaches the

234    target level $\omega_{\text{target}}$ during irrigation (default value = 1). In some cases, it can represent the

235    efficiency of the irrigation system, accounting for water losses due to evaporation, seepage, or

236    other factors.

237    The irrigation trigger threshold ($\omega_{\text{thresh}}$) in Equation (1) is calculated as:

$$238 \qquad \omega_{\text{thresh}} = f_{\text{thresh}}(\omega_{\text{trigger}} - \omega_{\text{wilt}}) + \omega_{\text{wilt}} \qquad (3)$$

239    where $\omega_{\text{trigger}}$ is the trigger water amount in the root zone (mm); $f_{\text{thresh}}$ is also a weighting

240    coefficient ranging from 0 to 1 that controls the proximity of soil water amount to the trigger

241    level $\omega_{\text{trigger}}$ (default value = 1). In this study, $f_{\text{irrig}}$ and $f_{\text{thresh}}$ were set to their default values.

242    The values of $\omega_{\text{trigger}}$ and $\omega_{\text{target}}$ are set according to the irrigation application method. For drip

243    and sprinkler irrigation, both $\omega_{\text{trigger}}$ and $\omega_{\text{target}}$ are set to the soil field capacity water amount. For

244    flood irrigation, $\omega_{\text{trigger}}$ is set to the soil field capacity water amount and $\omega_{\text{target}}$ to the saturation

245    water amount. For paddy irrigation, both $\omega_{\text{trigger}}$ and $\omega_{\text{target}}$ are set to the saturation water amount.

246    **2.2.2 Irrigation application**

247    The model incorporates four different irrigation application methods: drip irrigation, sprinkler

248    irrigation, flood irrigation, and paddy irrigation, each with unique triggering conditions, water

249    demand requirements, and application processes. Drip irrigation is triggered when soil moisture

250    in the root zone falls below field capacity, with the irrigation goal being to restore soil moisture

251    to field capacity. This method applies water directly to the surface soil, allowing it to percolate

252  into deeper soil layers. Sprinkler irrigation shares the same triggering condition and demand
253  requirement as drip irrigation but applies water above the canopy. In this method, water can be
254  intercepted and evaporated before reaching the soil surface, resulting in relatively lower
255  irrigation efficiency. This method is the most commonly used in the United States. Flood
256  irrigation is triggered when soil moisture falls below field capacity, to raise soil moisture to the
257  point of saturation. Paddy irrigation is applied whenever soil moisture drops below saturation,
258  aiming to restore soil moisture to saturation without causing runoff loss (Table S1). Paddy fields
259  are typically maintained with a specific water level on the surface (10 cm) during the growing
260  season. A global irrigation method map (Yao et al., 2022; Figure S4) is used to determine the
261  irrigation method for each grid. In addition, irrigation is implemented daily at 6 a.m., if
262  necessary, with water supply evenly distributed across each time step throughout the next 4
263  hours.

264  **2.2.3 Irrigation water supply/withdrawal**

265  The model incorporates two distinct irrigation water supply/withdrawal schemes. The first
266  scheme, Unlimited Supply (irrig-unlim), assumes that irrigation demand is fully met without
267  accounting for specific water sources, a common approach in most land surface models (Yao et
268  al., 2022). The second scheme, Limited Supply (irrig-lim), divides total irrigation demand
269  between surface water and groundwater sources, labeled as surface water demand ($D_{surf}$) and
270  groundwater demand ($D_{grnd}$), respectively. Both demands are constrained by the available water
271  within each respective system. This distribution is based on the spatial extent of groundwater
272  irrigation equipment, as provided by Siebert et al. (2010), and is formulated as follows:

$$D_{surf} = D_{irrig} \times (1 - f_{grnd}) \tag{4}$$

$$D_{grnd} = D_{irrig} \times f_{grnd} \tag{5}$$

275  where $D_{surf}$ and $D_{grnd}$ represent the demand from surface water and groundwater systems, and
276  $f_{grnd}$ denotes the area fraction covered by groundwater equipment. In this scheme, surface water
277  demand ($D_{surf}$) is sourced sequentially from local grid cell runoff, local river streamflow, and
278  upstream reservoirs, while groundwater demand ($D_{grnd}$) is drawn from groundwater aquifers.

279  **2.2.3.1 Surface water supply**

280  In our two-way coupled irrigation system (Figure 1), the daily surface water supply for irrigation
281  is constrained by surface water availability, which is simulated by CoLM (runoff) and CaMa-
282  Flood (local streamflow and upstream reservoirs). We first examine whether the runoff from the
283  local grid cell ($S_{ro}$) can meet the daily surface water demand ($D_{surf}$) for that cell. If runoff is
284  insufficient, additional water is sourced from local streamflow and upstream reservoirs. River

285  streamflow availability ($S_{riv}$) is determined by CaMa-Flood. For each irrigated grid cell, the river
286  grid with the highest flow within a 250 km radius is selected as the source. To prevent excessive
287  water extraction, a withdrawal limit is imposed, ensuring that the remaining flow in each river
288  grid cell does not drop below 20% of its average daily volume. Before conducting irrigation
289  simulations, natural river flow simulations are performed to establish essential parameters for
290  both river and reservoir water withdrawal schemes.

291  Reservoir water availability ($S_{res}$) is also determined by CaMa-Flood, which now includes a
292  reservoir module. This module consists of the following components: (i) a reservoir dataset that
293  provides reservoir location information matched with the river network, along with reservoir
294  parameters (e.g., characteristic storage capacity); (ii) a reservoir operation scheme designed for
295  flood control; and (iii) a routing scheme that integrates reservoir operations into river flow
296  simulations. For more details, refer to Hanazaki et al. (2022). In this study, we further propose a
297  new scheme for sourcing irrigation water from reservoirs (Figure 2), which involves the
298  following steps:

299  (i) Identifying the irrigation area served by each reservoir. It is challenging to accurately define
300  the true irrigation extent/area for each reservoir, especially across large spatial domains.
301  Therefore, a simplified approach is adopted here: larger reservoirs are assumed to cover a
302  proportionately larger irrigation area, restricted to downstream regions only (since upstream
303  water transfer is economically infeasible). Based on the relationship between reservoir size and
304  the corresponding irrigation area provided in Table S2, we calculate the irrigation area for each
305  reservoir according to its storage capacity by linear interpolation. Downstream irrigation grids
306  are selected sequentially, from nearest to farthest, until the cumulative grid area closely matches
307  the calculated irrigation area. If multiple reservoirs serve the same irrigation grid, a sharing
308  proportion ($f_{share}$, ranging from 0 to 1) is assigned to the irrigation grid based on the degree of
309  shared usage.

310  (ii) Calculating the irrigation demand for each reservoir by aggregating the demands of
311  associated irrigation grids. This is expressed as: $D_{res-total} = \sum_{i=1}^{N}\left(D_{irrig-unmet}^{i} \times f_{share}^{i}\right)$, where
312  $D_{irrig-unmet}^{i}$ and $f_{share}^{i}$ represent the irrigation demand (i.e., the portion of $D_{surf}$ not met by local
313  runoff and river streamflow) and sharing proportion of grid $i$, respectively. $N$ denotes the number
314  of irrigation grids served by the reservoir.

315  (iii) Executing reservoir withdrawals for irrigation based on demands. Water is then withdrawn
316  ($S_{res-total}$) from the reservoir's effective storage ($V_{eff}$) — the portion between the current water
317  level and dead water level—according to the required demand. This is expressed as
318  $S_{res-total} = \min(D_{res-total}, V_{eff})$. After updating the reservoir storage, the reservoir operation and
319  subsequent river routing are calculated following the approach outlined in Hanazaki et al. (2022).

320  (iv) Redistributing withdrawn water to the irrigation grids. Based on each irrigation grid's
321  contribution to the total reservoir irrigation demand, the total withdrawal volume is
322  proportionally allocated across the associated grids ($S_{res}^i$). This is expressed as

323  $S_{res}^i = S_{res\text{-}total} \times \frac{D_{irrig\text{-}unmet}^i \times f_{share}^i}{D_{res\text{-}total}}$. Notably, this water is not applied directly to irrigation but is stored in

324  a temporary reservoir (i.e., a temporary variable) for each irrigation grid in CoLM. This approach
325  addresses the response delay in water supply from the river routing model to the land model's
326  irrigation demands, as the time step for CoLM is 60 minutes, while CaMa-Flood operates with a
327  6-hour time step and exchanges information with CoLM every 6 hours. Moreover, if the
328  reservoir cannot fully meet the irrigation demand within the initial time step, any unmet demand
329  is carried forward to the next time step. This process continues over a 24-hour cycle, after which
330  new water demands for the next day are received.

331  Thus, the computational sequence proceeds as follows: Step (i) is completed before model
332  execution, with its results serving as an essential input for the irrigation module. During model
333  operation, CoLM calculates the irrigation demand at 6 a.m. local time. The unmet demand (after
334  subtracting the water supplied by local runoff and streamflow) is then sent to CaMa-Flood, as
335  described in Step (ii). CaMa-Flood supplies water from reservoir to meet this demand, as
336  described in Step (iii), and returns the supplied water to CoLM according to Step (iv), over the
337  next 24 hours. During this process, the water supplied by reservoir is stored in the temporary
338  reservoir (variable) for each irrigation grid within CoLM. The following day, when irrigation
339  begins again at 6 a.m., water is withdrawn directly from the temporary reservoir if the demand
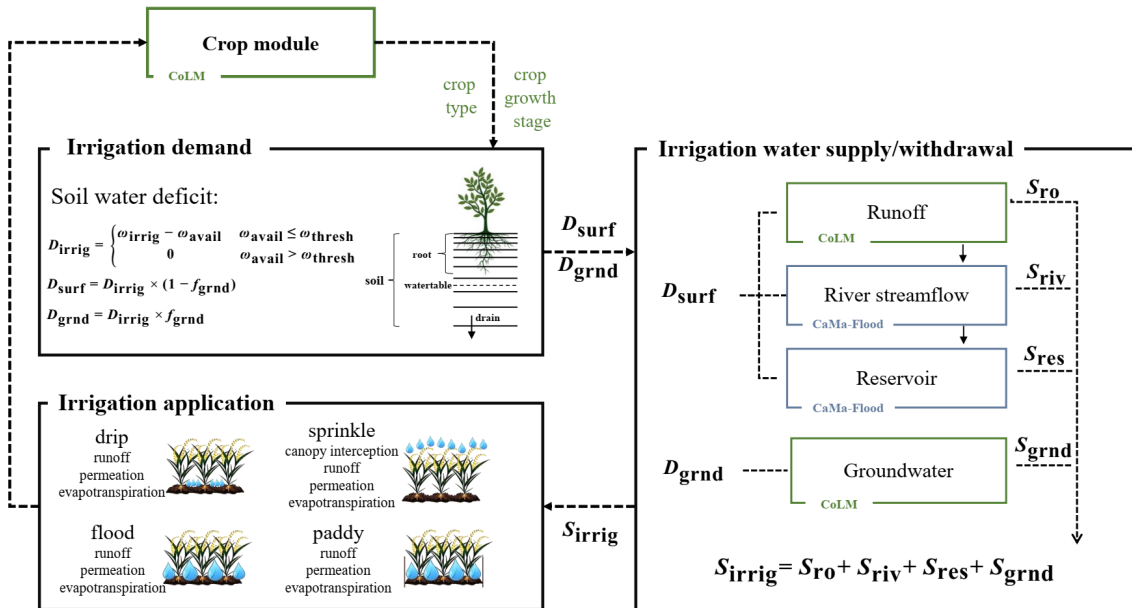340  cannot be met by local runoff and streamflow.

341



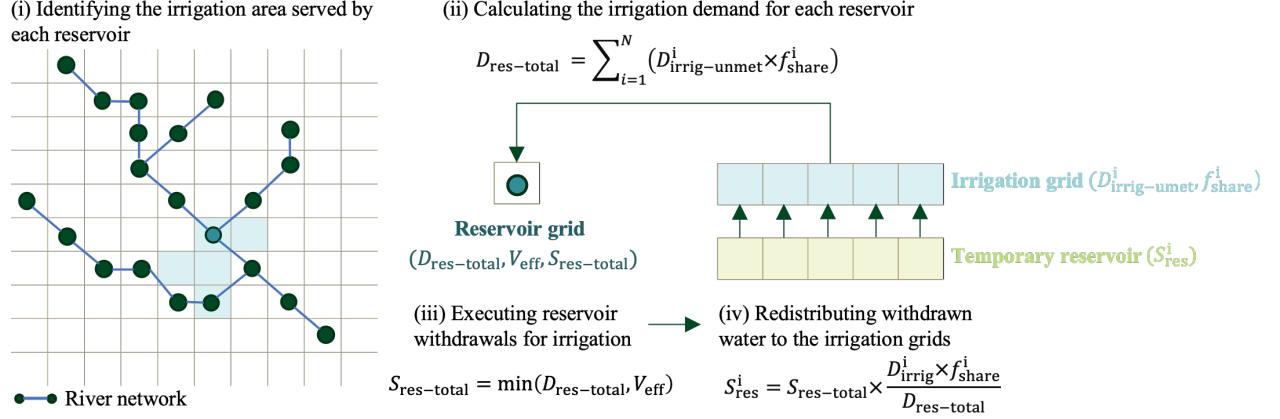342  **Figure 1.** Diagram of the two-way coupled irrigation water system in the Common Land Model.

**(i) Identifying the irrigation area served by each reservoir**

**(ii) Calculating the irrigation demand for each reservoir**

$$D_{\text{res}-\text{total}} = \sum_{i=1}^{N} \left( D^i_{\text{irrig}-\text{unmet}} \times f^i_{\text{share}} \right)$$

**Reservoir grid**
$(D_{\text{res}-\text{total}}, V_{\text{eff}}, S_{\text{res}-\text{total}})$

**Irrigation grid** $(D^i_{\text{irrig}-\text{umet}}, f^i_{\text{share}})$

**Temporary reservoir** $(S^i_{\text{res}})$

**(iii) Executing reservoir withdrawals for irrigation**

**(iv) Redistributing withdrawn water to the irrigation grids**

$$S_{\text{res}-\text{total}} = \min(D_{\text{res}-\text{total}}, V_{\text{eff}})$$

$$S^i_{\text{res}} = S_{\text{res}-\text{total}} \times \frac{D^i_{\text{irrig}} \times f^i_{\text{share}}}{D_{\text{res}-\text{total}}}$$

●—● River network

**Figure 2.** Diagram of the reservoir water supply scheme.

## 2.2.3.1 Groundwater supply

Groundwater supply is constrained by the availability of water within the aquifer. In CoLM, the groundwater table interacts with soil layers through vertical water exchange, allowing recharge or withdrawal of water from the aquifer (Li et al., 2017a). The evolution of the groundwater table is determined by the balance of soil water recharge and subsurface outflow, with the specific yield dynamically linking the water table position to changes in soil moisture and aquifer storage. When irrigation is required, water is directly extracted from the top of the simulated aquifer, and the water table depth is updated accordingly. This process continues until either the irrigation demand is fully met, or the water table falls below a predefined threshold, set as 1 meter below the initial depth at the beginning of the year (Jasechko et al., 2024; Russo and Lall, 2017). Groundwater supply is immediately available upon demand, with no temporal lag between the request and its availability for irrigation. Changes in the water table depth can then affect subsurface drainage and recharge from the bottom soil layer to the aquifer.

## 2.3 Materials

### 2.3.1 Input datasets

In this study, CoLM was implemented across the contiguous United States at a 0.25° spatial resolution for the period 2001–2016. Meteorological input data were derived from the WATCH Forcing Data methodology applied to ERA-Interim data (WFDEI) (Weedon et al., 2014), which has also been utilized in the Inter-Sectoral Impact Model Intercomparison Project Phase 2a (ISIMIP2a; Gosling et al., 2019). Soil property data were sourced from the Global Soil Dataset for Earth System Modeling (GSDE), originally provided at a spatial resolution of 30 arc-seconds (Dai et al., 2019; Shangguan et al., 2014). Land cover data were derived from the MODIS dataset (MCD12Q1; Friedl and Sulla-Menashe, 2022), providing detailed global land classification information at a spatial resolution of 500 meters.

369   The simulation of irrigation processes also required detailed data on crop areas, planting dates,
370   irrigation areas and irrigation methods. Crop planting areas were derived from the 30-meter
371   resolution CropScape and Cropland Data Layer (CDL) datasets (2008–2020) and aggregated to a
372   spatial resolution of 5 arcminutes for analysis (USDA, 2019). These datasets, produced by the
373   U.S. Department of Agriculture, provide annual, crop-specific land cover information using
374   satellite imagery and ground reference data. For each pixel, we calculated the proportion of
375   cropland relative to the pixel's area (PCT_CROP) and the proportions of maize, wheat, and
376   soybean relative to the cropland area (PCT_CFT). Pixels with a cropland percentage
377   (PCT_CROP) exceeding zero were classified as crop pixels. The Plant Functional Type (PFT)
378   approach employed in CoLM allowed different crops and vegetation types coexist within the
379   same grid cell according to their percentages (PCT_CFT). To define planting and harvesting
380   dates, we utilized an observation-based crop calendar dataset from the Global Gridded Crop
381   Model Intercomparison (GGCMI), which provided information for 20 major crops under both
382   rainfed and irrigated conditions at each grid cell for 1980–2010 (Jägermeyr et al., 2021).

383   The irrigation map was derived using the 5' resolution data from the FAO Global Map of
384   Irrigation Areas - Version 5 (Siebert et al., 2013). Since the CropScape data does not distinguish
385   between rainfed and irrigated crops, we combined it with the irrigation map to determine the
386   proportions of rainfed and irrigated crops. Irrigation water withdrawals were classified into
387   surface water and groundwater sources following FAO data on regions equipped for groundwater
388   extraction, which informed the allocation of irrigation demand across sources (Siebert et al.,
389   2010). The irrigation application method data was obtained from Yao's global irrigation map,
390   which details irrigation methods (drip, sprinkler, or flood) for 32 crop types, each assigned a
391   single method (Yao et al., 2022). Jägermeyr et al. (2015) originally used a decision tree to refine
392   AQUASTAT's data, classifying irrigation methods for 14 Crop Functional Types (CFTs) based
393   on crop area, soil characteristics, and socio-economic conditions. Yao et al. (2022) then matched
394   these CFTs to 32 crop types in CLM5 and incorporated an additional irrigation method, *paddy*,
395   specifically for rice-growing regions, creating a more detailed global irrigation dataset.

396   For river routing simulations in CaMa-Flood, the baseline topography was derived from the
397   Multi-Error-Removed Improved-Terrain Hydrography dataset (MERIT Hydro; Yamazaki et al.,
398   2019). Fundamental information on dams/reservoirs in the river network, including dam name,
399   coordinates, total storage capacity, and drainage area, was obtained from the GRanD database
400   (Lehner et al., 2011). GRanD version 1.3 contains data on 7,320 dams globally, along with their
401   associated reservoirs. The locations of the dams in the 0.25° river map were determined
402   following the method outlined by Hanazaki et al. (2022), which enabled the identification of
403   1464 reservoirs across the contiguous United States (Figure S3). In addition to GRanD, the
404   Global Reservoir Surface Area Data Set (GRSAD; Zhao and Gao, 2018) and the Global
405   Reservoir Geometry Database (ReGeom; Yigzaw et al., 2018) were used to estimate reservoir
406   parameters, such as storage capacity at emergency, flood control, and critical levels (Hanazaki et
407   al., 2022). GRSAD provides a monthly time series of surface areas for 6,817 GRanD reservoirs

408  from 1984 to 2015, based on global surface water occurrence data (Pekel et al., 2016). ReGeom
409  contains storage-area-depth information for 6,824 reservoirs in GRanD, with geometry estimates
410  derived from assumed surface and cross-sectional shapes, as well as data on reservoir extent,
411  total storage, and surface area.

412  **2.3.2 Validation datasets**

413  To evaluate the scheme developed in this study, we focused on validating irrigation water
414  withdrawal volumes, land fluxes (including energy fluxes and river flows) and crop yields in
415  irrigated areas. We used hydrological survey data from the U.S. Geological Survey (USGS,
416  2023), which provided detailed statistics on total irrigation water withdrawals, categorized by
417  surface and groundwater sources, every five years since 2000. Within the timeframe of this
418  study, data were available for the years 2005, 2010, and 2015. Building on this, Ruess et al.
419  (2024) employed a global hydrological model (PCR-GLOBWB) to estimate annual, crop-
420  specific irrigation water withdrawals from 2008 to 2020. Additionally, we compared the
421  irrigation water withdrawal volumes simulated by our model with those generated by six other
422  hydrological models—VIC, PCR-GLOBWB, MATSIRO, LPJmL, H08, and DBH—that
423  participated in ISIMIP2a (Gosling et al., 2019). Although more hydrological models were
424  included in ISIMIP2a, our comparison was limited to these six because they provided irrigation
425  water withdrawal outputs. The simulations were driven by the WFDEI climate dataset, with a
426  spatial resolution of 0.5° and covering the period from 1971 to 2010.

427  For land surface flux validation, we used monthly latent and sensible heat fluxes provided by
428  FLUXCOM at a resolution of 0.5° (Jung et al., 2019). FLUXCOM leveraged FLUXNET site
429  observations and extended these globally through machine learning algorithms, resulting in a
430  global dataset for latent heat, sensible heat, and carbon fluxes. For temperature validation, we
431  used land surface temperature data from 2001 to 2016 at a spatial resolution of 0.1° from the
432  ERA5-Land reanalysis dataset (Muñoz-Sabater et al., 2021).

433  For streamflow validation, we utilized monthly streamflow data from the Global Runoff Data
434  Centre (GRDC, 2023) for the period 2001–2016. To ensure robust validation, we excluded
435  catchments with fewer than five years of data during the study period and focused on catchments
436  significantly influenced by irrigation while minimizing the impacts of other anthropogenic
437  activities. These selection criteria ultimately resulted in 77 catchments being included in the
438  analysis (Figure S10).

439  For terrestrial water storage (TWS) validation, we utilized monthly terrestrial water storage
440  anomaly data from the Gravity Recovery and Climate Experiment (GRACE) mission for the
441  period 2002-2016, with a spatial resolution of 0.5 degree, provided by the NASA Jet Propulsion
442  laboratory (Watkins et al., 2015; Wiese et al., 2016).

443  For crop yield validation, we relied on annual yield reports for irrigated and rainfed crops from
444  the USDA NASS at the county level, which is regarded as a reliable source of yield statistics
445  (USDA/NASS, 2023). The data for irrigated crops primarily covered the Central Plains of the
446  United States, with limited coverage in the eastern and western regions. We aggregated our grid-
447  based yield simulation results to the county level and performed validation only for regions and
448  years with available USDA data.

## 2.4 Experimental Design

450  This study conducted three simulation experiments to evaluate the effectiveness of the newly
451  developed module by comparing their performance: (i) Non-Irrigation Experiment (abbreviated
452  as noirrig): This scenario assumes all crops in the region are rainfed, with no irrigation applied. It
453  serves as a baseline to represent natural surface water and energy balance conditions. (ii)
454  Unlimited Irrigation Experiment (abbreviated as noirrig-unlim): This scenario distinguishes
455  between irrigated and rainfed areas based on crop maps. In irrigated areas, crop water demands
456  are fully satisfied throughout the growing season, without considering the limitations of water
457  resources. (iii) Limited Irrigation Experiment (abbreviated as irrig-lim): In this scenario,
458  irrigation water is supplied proportionally from surface water and groundwater based on
459  availability, as illustrated in Figure 1. Here, irrigation is constrained by the availability of surface
460  and groundwater, which may result in unmet crop water demands.

461  The non-irrigation experiment was first simulated for the period 2001–2010 to stabilize
462  vegetation carbon and nitrogen pools, soil moisture, and the groundwater table. This stabilized
463  state served as the initial condition for all three experiments. The main simulation period spanned
464  2001-2016, covering the contiguous United States at a spatial resolution of 0.25° × 0.25°. In the
465  subsequent analysis, key evaluation metrics—bias, root-mean-square error (RMSE), Pearson
466  correlation coefficient ($r$), and Kling-Gupta efficiency (KGE)—were employed to assess the
467  performance of the simulations.

468  **Table 1.** Experiment Configurations.

| Experiment | Management | Water limitation | Water sources |
|---|---|---|---|
| noirrig | Rainfed | NA | NA |
| irrig-unlim | Irrigated | No | NA |
| irrig-lim | Irrigated | Yes | Surface water and groundwater |

## 3. Results

### 3.1 Evaluation of simulated irrigation water withdrawal

### 3.1.1 Comparison with observations

Based on annual irrigation withdrawal data from the USGS, states in the western and central United States withdraw significantly more water for irrigation than those in the eastern regions (Figure 3a). This is primarily due to the relatively low precipitation in the western and central regions, where the majority of irrigated areas are located, while crops in the eastern U.S. are predominantly rainfed. The top five states with the highest annual irrigation withdrawals— California (CA), Idaho (ID), Colorado (CO), Arkansas (AR), and Montana (MT)—are all situated in the Midwest and West (Figure 3b). Nationally, the total annual irrigation withdrawal averages approximately 166.23 $km^3 yr^{-1}$, based on data from 2005, 2010 and 2015. In comparison, the irrig-unlim and irrig-lim schemes simulate national total withdrawals of 290.94 $km^3 yr^{-1}$ and 120.81 $km^3 yr^{-1}$, respectively. As illustrated in Figure 3c-f, the simulations capture the spatial patterns of water withdrawals across different states effectively, with the irrig-lim scheme yielding better performance. The root-mean-square-error (RMSE) and correlation coefficient ($r$) for the irrig-lim scheme are 3.60 $km^3 yr^{-1}$ and 0.82, respectively, slightly outperforming the corresponding values for the irrig-unlim scheme (9.78 $km^3 yr^{-1}$ and 0.76).

Irrigation water withdrawals draw from both surface water and groundwater sources. According to USGS reports, most irrigation withdrawals in the central U.S. come from groundwater (Dieter et al., 2018). In states such as Missouri (MO), Kansas (KS), Iowa (IA), Illinois (IL), Rhode Island (RI), and Mississippi (MS), the share of groundwater withdrawals exceeds 90% (Figure 4c). In contrast, states with high surface water withdrawals are primarily in the eastern and western U.S., with states like Wyoming (WY), Connecticut (CT), Kentucky (KY), and Montana (MT) reporting surface water withdrawal proportions greater than 90%. These spatial variations in water source usage are primarily attributed to the central U.S.'s abundant groundwater resources and widespread groundwater extraction infrastructure.

In our simulations, the irrig-lim scheme effectively accounts for irrigation water withdrawals from different sources, constrained by their availability. Encouragingly, the scheme generally reproduces observed annual surface water and groundwater withdrawals across states (Figure 4a-b), achieving correlation coefficients of 0.68 and 0.95, respectively. Furthermore, the simulated proportions of water sources closely align with observed data (Figure 4c-d), with a correlation coefficient of 0.64 ($p < 0.01$). However, the model tends to underestimate the surface water withdrawal proportions in the northwestern regions of the U.S. (particularly in Montana and Colorado; Figure 4d), while slightly overestimating them in some central and eastern states. This discrepancy may stem from limitations in the data used to allocate water demand. Specifically, the model relies on pre-determined groundwater extraction infrastructure proportions, which may

not accurately reflect actual extraction practices, particularly as the dataset was published in
2005 and may not account for subsequent changes in groundwater infrastructure in certain states.
Alternatively, the discrepancy could arise from model biases in simulating surface and
groundwater availability. For example, in the northwestern region, surface runoff is heavily
influenced by snowmelt and glacial meltwater (Li et al., 2017b), and biases in simulating these
processes could lead to an underestimation of surface water availability.
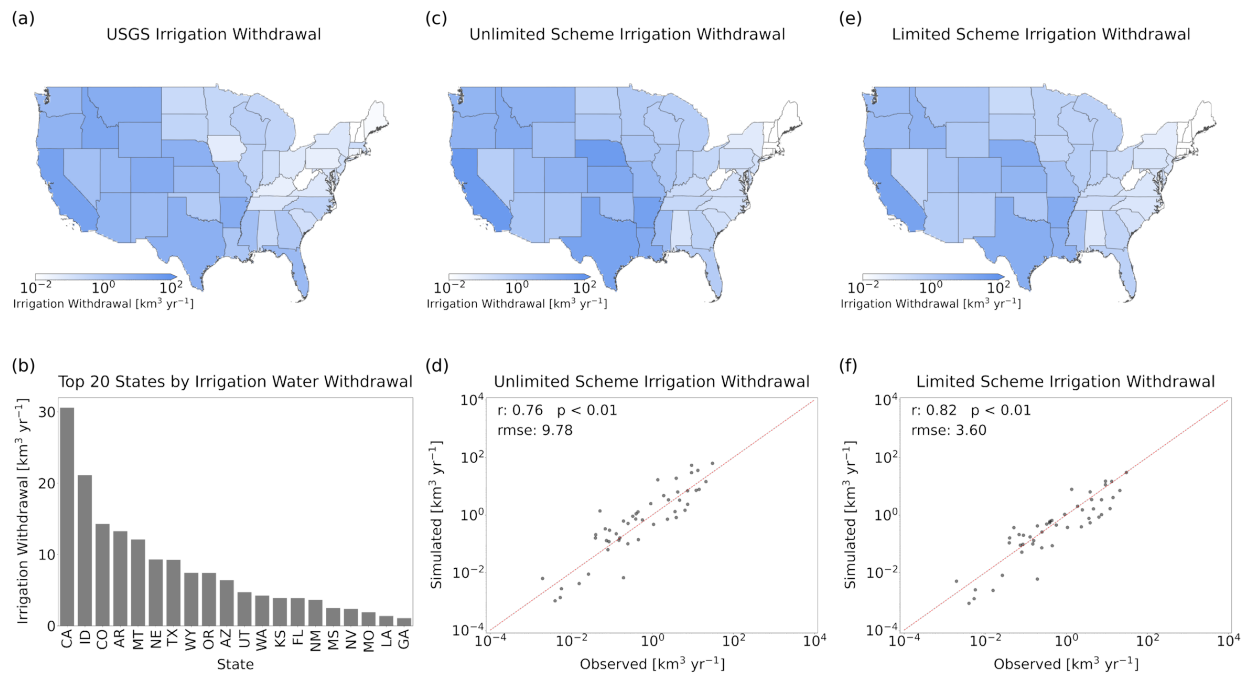


**Figure 3.** Comparison of reported and simulated irrigation water withdrawal in the United States.
(a) Annual irrigation water withdrawal reported by the USGS for individual states. (b) Annual
withdrawal amounts for the top 20 states by irrigation water withdrawal. (c) Annual irrigation
water withdrawal simulated by CoLM using the unrestricted water supply (irrig-unlim) scheme
for individual states. (d) Comparison of reported and simulated irrigation water withdrawal
(using the irrig-unlim scheme) for individual states, with Pearson correlation coefficient (*r*) and
root mean square error (RMSE) displayed, along with statistical significance (two-tailed
Student's t-test). (e) Annual irrigation water withdrawal simulated by CoLM using the restricted
water supply (irrig-lim) scheme for individual states. (f) Comparison of reported and simulated
irrigation water withdrawal (using the irrig-lim scheme) for individual states.

(a) Limited Scheme Surface Water Withdrawal

(b) Limited Scheme Ground Water Withdrawal

(c) Observed Surface Water Supply Ratio
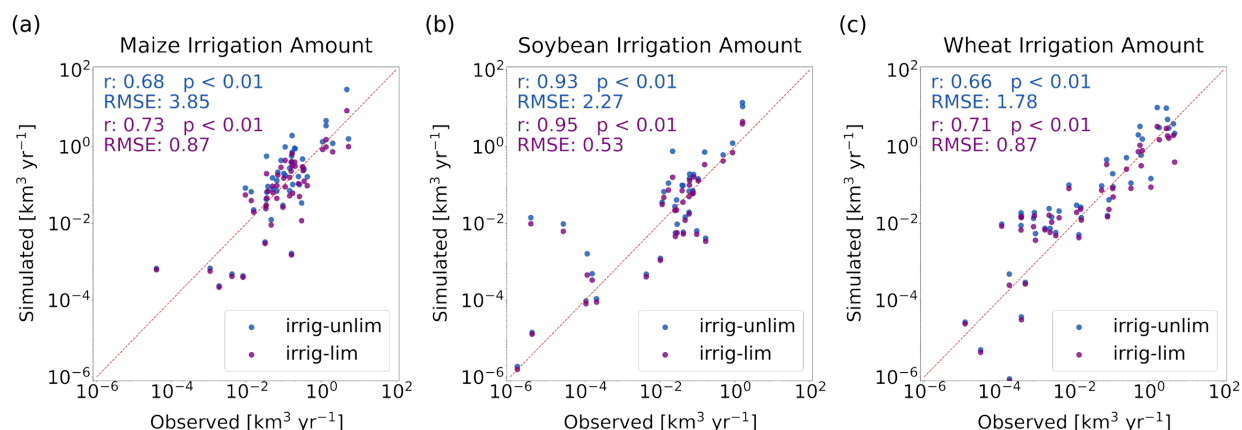
(d) Simulated Surface Water Supply Ratio
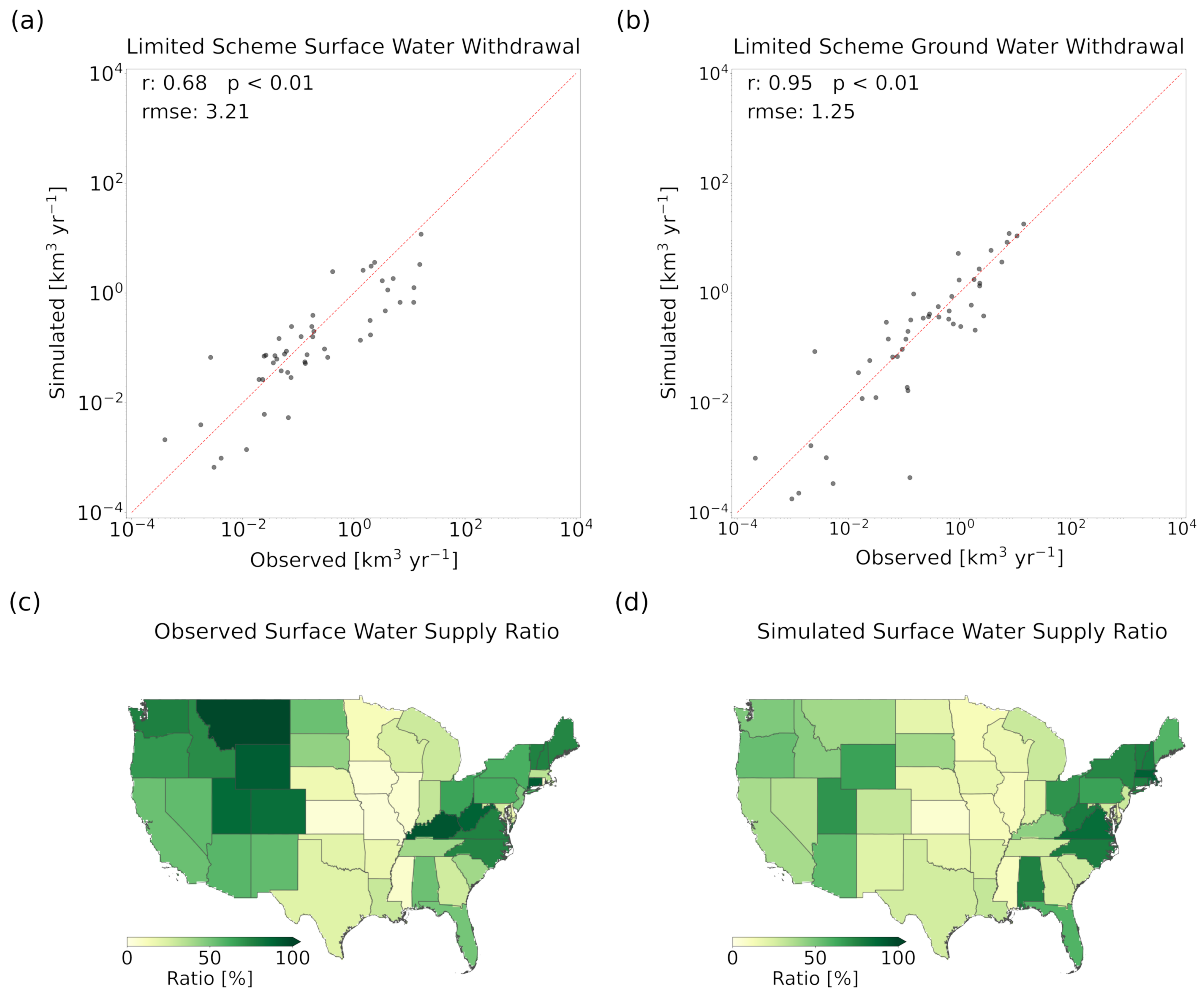
**Figure 4.** Comparison of reported and simulated irrigation water withdrawal in the United States by water source. (a) Comparison of reported and simulated surface water withdrawal volumes for individual states. (b) Same as (a), but for groundwater withdrawal volumes. (c) Proportion of surface water in irrigation withdrawal, based on USGS reports for individual states. (d) Proportion of surface water in irrigation withdrawal, simulated by CoLM using the irrig-lim scheme for individual states.

Ruess et al. (2024), using data from the USGS and model outputs from PCR-GLOBWB 2, generated an irrigation water withdrawal dataset that included withdrawal volumes for major crops in the U.S. According to this dataset (Figure 5), wheat is the largest consumer of irrigation water, with an average annual withdrawal of approximately 27.29 $km^3$ $yr^{-1}$, followed by maize at about 20.91 $km^3$ $yr^{-1}$. In contrast, soybean requires considerably less irrigation (i.e., 5.89 $km^3$ $yr^{-1}$), partly due to its greater drought tolerance and smaller planted area compared to the other two crops. Under the irrig-unlim (irrig-lim) simulation scheme, the annual irrigation withdrawals for maize, wheat, and soybean are 53.98 $km^3$ $yr^{-1}$, 47.53 $km^3$ $yr^{-1}$, and 29.99 $km^3$ $yr^{-1}$ (19.19 $km^3$ $yr^{-1}$,

17

537    17.95 km³ yr⁻¹, and 11.05 km³ yr⁻¹), respectively. Once again, the irrig-lim scheme provides a
538    closer alignment with observation-based data, as indicated by a lower RMSE (Figure 5). These
539    results suggest that our irrigation module generally performs well in simulating total national
540    annual water withdrawals, the spatial distribution of withdrawals (Figure 3), the proportion of
541    water source types (Figure 4), and the irrigation volumes for different crops (Figure 5).



542

**Figure 5.** Comparison of reported and simulated irrigation water withdrawal in the United States
by crop type. (a) Comparison of reported and simulated irrigation water withdrawal for maize,
using both the unrestricted (irrig-unlim, blue dots) and restricted (irrig-lim, purple dots) supply
schemes for individual states. (b-c) Same as (a) but for soybean and wheat.

### 3.1.2 Comparison with other models

548    We further compare the irrigation water withdrawal simulations from this study with outcomes
549    from six global hydrological models (VIC, PCR-GLOBWB, MATSIRO, LPJmL, H08, and
550    DBH) that participated in ISIMIP2a. Notably, all simulations used the same climate forcing
551    (WFDEI), ensuring consistency in the comparison. Our results, particularly from the irrig-lim
552    scheme, closely align with observed total national annual irrigation withdrawals. By contrast,
553    five of the six models, excluding LPJmL, exhibit larger absolute deviations from observed value
554    (Figure 6a). Regarding spatial distribution, most models perform well (Figure 6b), with LPJmL
555    (orange dots) achieving the highest correlation coefficient (0.89) and the lowest RMSE (2.86 km³
556    yr⁻¹). The irrig-lim scheme in this study (purple dots) performs comparably to LPJmL,
557    demonstrating competitive accuracy. In terms of temporal dynamics, comparisons across models
558    are limited due to the scarcity of observed data. However, the general seasonal patterns are
559    consistent across models (Figure S6), with the highest irrigation withdrawals occurring in June
560    and July, and the lowest in January and December. Most models exhibit similar seasonal
561    fluctuations, with irrigation volumes during peak months approximately ten times greater than
562    during off-peak months. Overall, these results suggest that our model performs similarly to, or
563    even better than, existing models in simulating irrigation water withdrawals in the U.S.
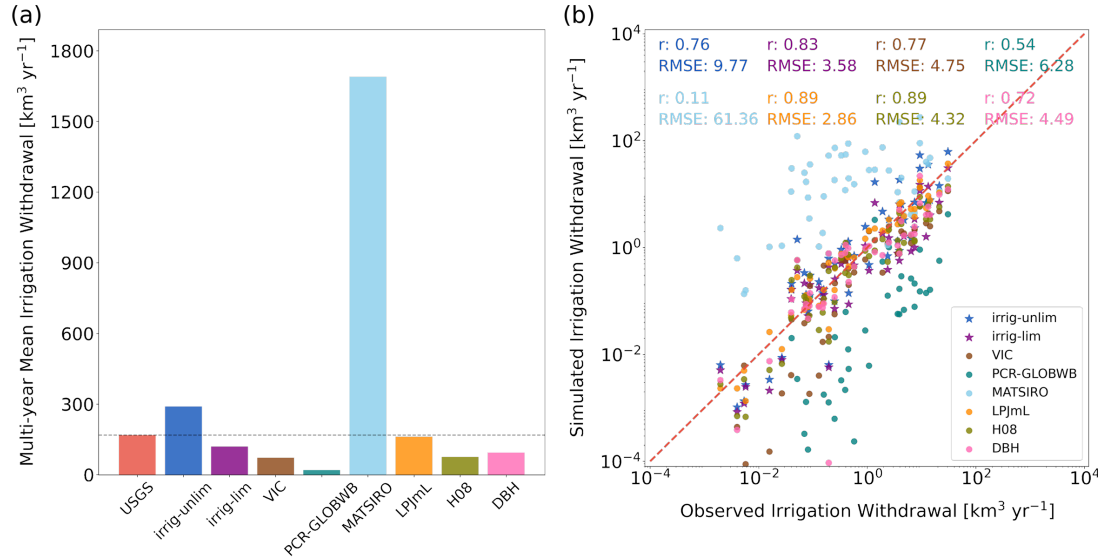
18

**Figure 6.** Comparison of irrigation water withdrawal simulated by CoLM and six global hydrological models participating in ISIMIP2a. (a) Annual total irrigation water withdrawal amounts in the United States as reported by the USGS, compared with simulations from CoLM (using both the irrig-unlim and irrig-lim schemes) and the six global hydrological models. (b) Comparison of reported and simulated irrigation water withdrawal for individual states, with Pearson correlation coefficient ($r$) and root mean square error (RMSE) for each simulation displayed.

## 3.2 Evaluation of simulated land energy and water fluxes

### 3.2.1 Evaluation of simulated energy fluxes

We evaluate CoLM's performance in simulating surface energy fluxes over irrigated areas in the U.S. using different schemes, with FLUXCOM monthly sensible heat (*SH*) and latent heat (*LH*) fluxes as observational references. Figure 7 compares multi-year monthly averages of observed and simulated *SH* and *LH* fluxes across irrigated grid points. Without irrigation (the noirrig scheme), the model significantly overestimates *SH* (Figure 7a) with an average bias of 16.89 W m$^{-2}$ (44.53%) and underestimates *LH* (Figure 7c) with an average bias of 18.84 W m$^{-2}$ (37.11%). In contrast, biases over non-irrigated grids are considerably lower, at 3.04% and 17.38% for *SH* and *LH*, respectively (Figure S7). This indicates that CoLM performs satisfactorily in simulating energy processes over natural vegetation and rainfed areas, but less so over irrigated regions.

With the inclusion of the irrigation module, simulation errors in surface energy fluxes over irrigated areas are significantly reduced, particularly in the U.S. High Plains and the California Central Valley (Figures S8 and S9). Under the irrig-unlim and irrig-lim schemes, average *SH* biases decrease to 27.10% and 30.79%, respectively, while *LH* biases decrease to 18.41% and 22.18%. These improvements are evident across most irrigated grid points, as illustrated by the

19

588  KDE curves of KGE, which indicate an increase in grid points with higher KGE values (Figure
589  7). A KS test confirms that the differences between the irrigation (i.e., the irrig-unlim and irrig-
590  lim schemes) and noirrig simulations are statistically significant. Although the irrig-unlim
591  scheme performs slightly better than irrig-lim for *SH* and *LH*, this difference is not significant.
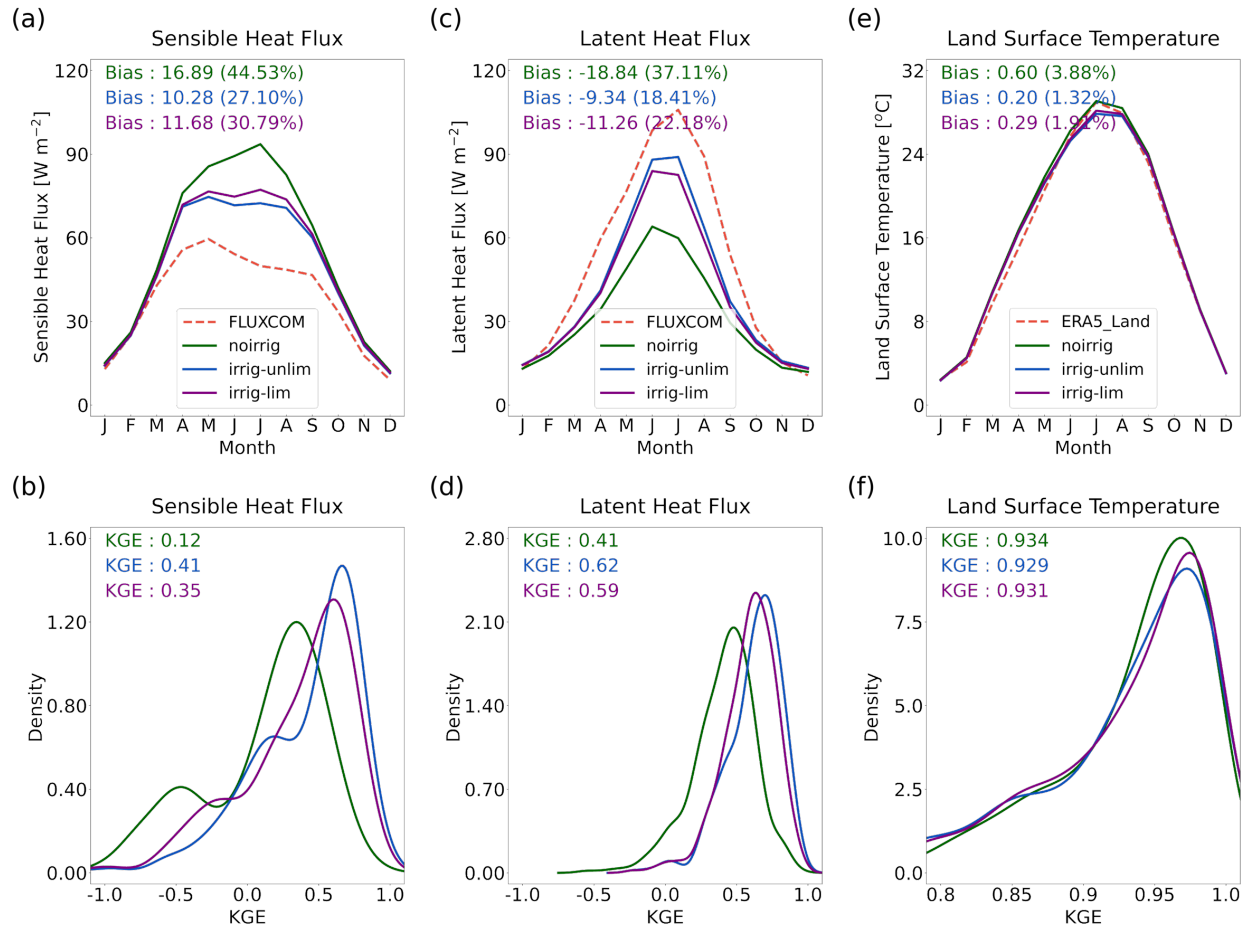


**Figure 7.** Evaluation of simulated energy fluxes and land surface temperature in the irrigation
region. (a) Monthly sensible heat flux averaged from 2001 to 2016, based on FLUXCOM dataset
and simulated by CoLM using the noirrig, irrig-unlim, and irrig-lim schemes in irrigation regions
of the United States, with the bias between simulations and observations (i.e., FLUXCOM)
indicated in the panel. (b) Kernel density estimate (KDE) curves for the Kling-Gupta efficiency
(KGE) between observed and simulated monthly sensible heat flux for each irrigation grid, with
mean KGE value indicated in the panel. (c-d) Same as (a-b) but for latent heat flux. (e-f) Same as
(a-b) but for land surface temperature, using data from ERA5-Land reanalysis dataset.

601  Additionally, the FLUXCOM data (red dashed line) show that the highest monthly *SH* and *LH*
602  occur in May and July, respectively. However, the noirrig simulation (green solid line) fails to
603  capture this seasonal peak, showing instead that *SH* peaks in July and *LH* in June. This
604  discrepancy is not present in non-irrigated areas (Figure S7), suggesting that irrigation in

20

605  agricultural regions (and the subsequent crop growth it supports) substantially affects the
606  seasonal pattern of regional energy balance. When the irrigation module is incorporated into the
607  model, these seasonal patterns are more accurately reproduced, with the timing of the simulated
608  peak months aligning more closely with FLUXCOM data (blue and purple solid lines).

609  The incorporation of the irrigation module improves the simulation of energy partitioning in
610  irrigated areas, enabling the model to better capture surface temperature dynamics (Figure 7e).
611  Under the noirrig scheme, the average bias of monthly surface temperature is 0.6℃° (3.88%).
612  This bias decreases to 0.20℃° (1.32%) with the irrig-unlim scheme and 0.29℃° (1.91%) with the
613  irrig-lim scheme. However, even with irrigation included, the simulated total evapotranspiration
614  remains systematically underestimated (Figure 7c). This underestimation is also evident in non-
615  crop areas (Figure S7c), suggesting that it may not be due to limitations in the irrigation module
616  itself but rather to certain deficiencies in CoLM's evapotranspiration simulation approach.

**3.2.2 Evaluation of simulated river flow**

618  Irrigation processes can significantly alter natural hydrological dynamics and river flow patterns
619  both temporally and spatially. To evaluate the effectiveness of the irrigation module in capturing
620  these impacts, we compare model outputs with observed catchment streamflow data. We select
621  catchments that are substantially influenced by irrigation while minimizing the effects of other
622  anthropogenic activities. Figure S10 illustrates the locations of the selected 77 catchments.
623  Figure 8 shows that CoLM's performance in simulating runoff—and consequently streamflow—
624  remains limited, with relatively low average KGE values across all three schemes. This
625  limitation is likely due to the use of a simplified runoff parameterization scheme in CoLM (Li et
626  al., 2011). However, it is encouraging to note that the irrig-lim scheme notably improves monthly
627  streamflow simulations compared to the noirrig scheme, increasing the average KGE from -0.57
628  to -0.49 and reducing the average percentage bias (PBIAS) from 117.28% to 106.54%. The
629  enhancement can be largely attributed to the incorporation of irrigation effects, which account
630  for reduced streamflow due to increased water use for evapotranspiration. This adjustment
631  effectively mitigates the overestimation of streamflow observed in the noirrig scheme.

632  Our analysis reveals that the irrig-unlim scheme significantly reduces the accuracy of streamflow
633  simulations compared to the noirrig scheme, leading to a pronounced overestimation of river
634  discharge. This issue arises because the irrig-unlim scheme meets any irrigation demand by
635  introducing additional water directly into the system without considering its source. Such an
636  approach is common among crop and land surface models that incorporate irrigation (Malek et
637  al., 2017; Yao et al., 2022; Zhang et al., 2020b). However, our findings indicate that introducing
638  extra water for irrigation without accounting for its specific sources and limitations may lead to
639  an imbalance in the water budget from a comprehensive perspective of the entire water system,
640  undermining the model's ability to accurately represent the dynamics of the hydrological system.
641  Furthermore, we compared observed and simulated monthly streamflow in ten larger catchments

(Figure S12), providing a more intuitive assessment. The results clearly indicate that the irrig-lim
643 scheme produces streamflow estimates that align more closely with observations, whereas the
644 irrig-unlim scheme tends to overestimate streamflow, particularly during months with high
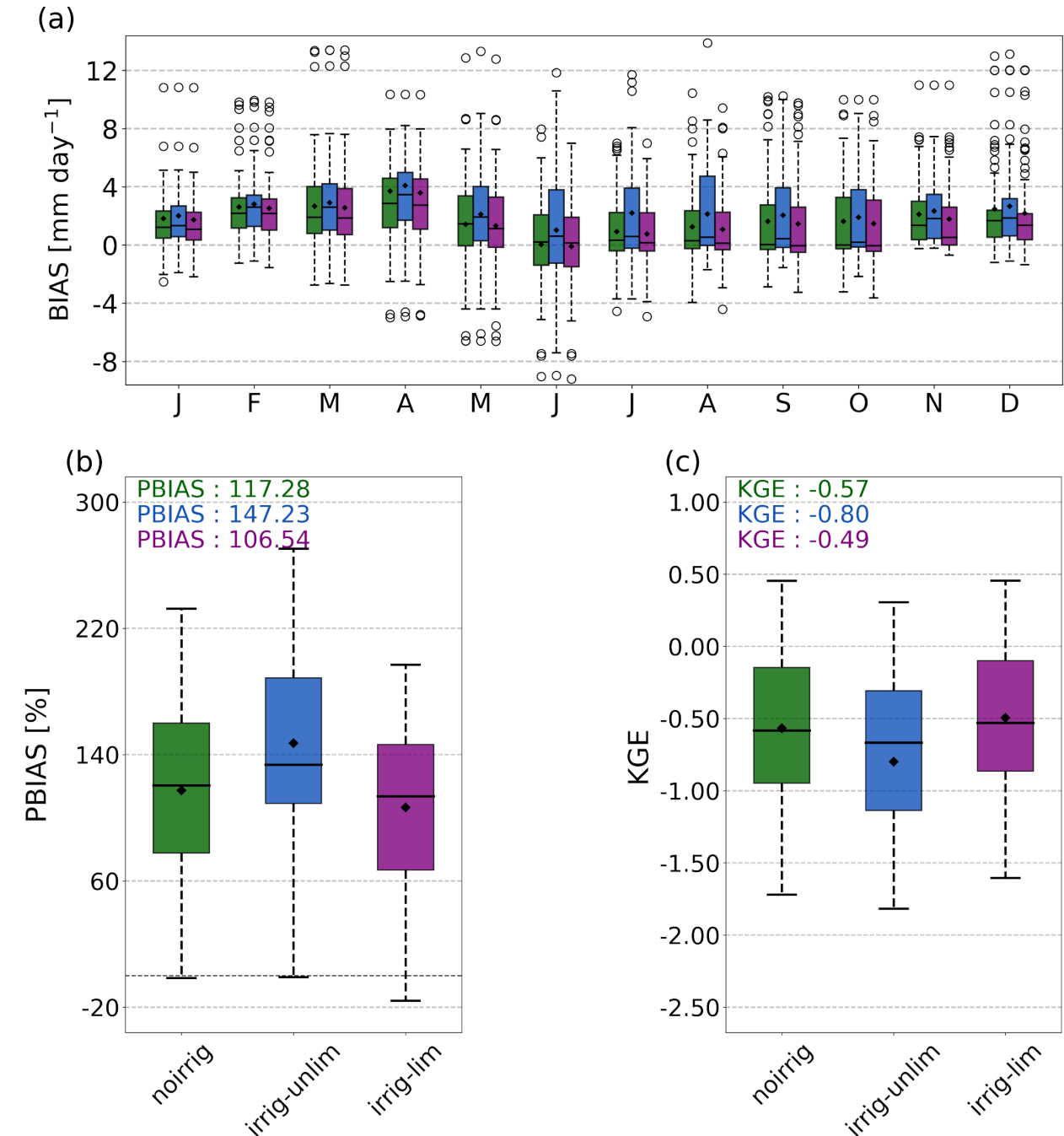645 irrigation demand.

(a)



(b)

PBIAS : 117.28
PBIAS : 147.23
PBIAS : 106.54

(c)

KGE : -0.57
KGE : -0.80
KGE : -0.49

646
647 **Figure 8.** Evaluation of simulated streamflow in 77 irrigation-affected catchments. (a) Multi-
648 year average monthly streamflow bias simulated using the noirrig, irrig-unlim, and irrig-lim
649 schemes in the evaluation catchments. The boxes represent the interquartile range, black lines

650      indicate median values, black dots show mean values, and dashed black whiskers extend to 1.5
651      times the interquartile range; points outside the boxes represent outliers. (b) Percentage bias
652      (PBIAS) between observed monthly streamflow and simulations from CoLM under the noirrig,
653      irrig-unlim, and irrig-lim schemes, with the average PBIAS value indicated in the panel. (c)
654      Same as (b) but for the Kling-Gupta efficiency (KGE) between simulated and observed
655      streamflow.

### 3.2.3 Evaluation of simulated terrestrial water storage anomalies

657      To assess the model's ability to simulate the impact of irrigation on terrestrial water storage
658      (TWS) dynamics, we compared the simulated monthly TWS anomalies with those derived from
659      GRACE satellite products provided by the NASA Jet Propulsion laboratory. The results showed
660      that incorporating the irrigation module, particularly under the irrig-lim scheme, improved the
661      model's ability to capture both the interannual variability (Figure 9a) and seasonal patterns
662      (Figure 9b) of TWS anomalies. Under the noirrig scheme, the simulated monthly TWS
663      anomalies from 2002 to 2016 had a Pearson correlation of 0.25 with GRACE data and an RMSE
664      of 6.75. In contrast, the irrig-lim scheme increased the correlation to 0.75 and reduced the RMSE
665      to 5.13 (Figure 9a). The spatial distribution of Pearson correlation coefficients between the
666      simulations and GRACE data (Figure S13) further demonstrated a widespread improvement
667      across the U.S., particularly in the Corn Belt.

668
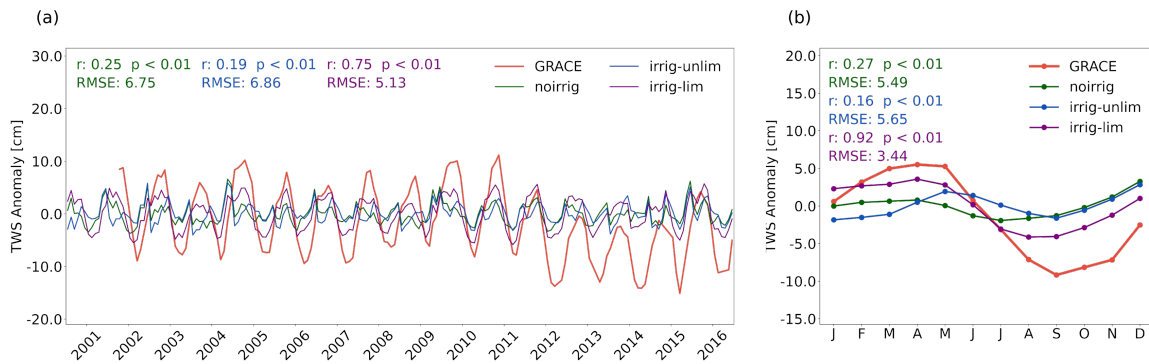
**Figure 9.** Evaluation of simulated terrestrial water storage anomalies in irrigated region. (a) Time
series of monthly terrestrial water storage anomalies from 2001 to 2016, simulated by CoLM
(under the noirrig, irrig-unlim, and irrig-lim schemes) and derived from GRACE (JPL dataset).
The Pearson correlation coefficient (r) and root mean square error (RMSE) between the
simulations and GRACE data are indicated in the panel. (b) Climatological monthly terrestrial
water storage anomalies averaged over 2001–2016, simulated by CoLM and derived from
GRACE.

676      The enhancement was even more pronounced in the simulation of seasonal TWS anomaly
677      patterns. Without irrigation, the model underestimated seasonal variations, resulting in a pattern

23

678 that deviated substantially from GRACE observations. This bias was effectively corrected in the
679 irrig-lim scheme, where the Pearson correlation coefficient increased to 0.92 and the RMSE
680 decreased to 3.44 (Figure 9b). However, none of the simulations captured the decline in
681 GRACE-derived TWS anomalies during 2012 to 2016, likely due to groundwater depletion from
682 irrigation (Rodell and Reager, 2023). This suggests that the model may require further validation
683 and improvements in simulating irrigation-induced groundwater storage changes.

## 3.3 Evaluation of simulated crop yield

685 Irrigation reflects a direct human influence on crop yields by providing supplemental water. Crop
686 models primarily focus on this aspect, but they often neglect how irrigation affects other
687 processes. Conversely, most hydrological models concentrate on the impact of irrigation
688 withdrawals on the water cycle, with some also addressing energy fluxes, yet pay less attention
689 to crop yield. From this perspective, land surface models offer distinct advantages; they provide
690 a more detailed representation of hydrological and surface energy processes compared to crop
691 models, while also presenting more physics-based representations of crop growth than traditional
692 hydrological models. Therefore, this study further evaluates whether incorporating the developed
693 irrigation module can enhance crop yield the simulations.

694 Using county-scale crop yield data for irrigated and rainfed regions provided by the USDA, we
695 assess simulated yields under both irrigated and non-irrigated scenarios. The dataset may not
696 comprehensively cover all irrigated areas in the U.S. or all years during the study period, so
697 comparisons are limited to regions and years with reported data. In rainfed regions, the model
698 broadly reproduces average annual yields for the maize, soybean, and wheat (Figure S14).
699 However, in irrigated regions, the model without irrigation significantly underestimates crop
700 yields, with average underestimations of 31.95%, 44.45%, and 35.95% for maize, soybean, and
701 wheat, respectively (Figure 10). Under both the irrig-umlim and irrig-lim schemes, despite slight
702 differences in performance across crops, the model effectively simulates yield increases under
703 irrigation, aligning well with observations. As shown in Figure S15, the yield underestimation
704 observed in most counties without irrigation is substantially corrected under the irrig-unlim (and
705 irrig-lim) schemes, with 90.5% (70.8%), 99.5% (94.2%), and 68.4% (74.8%) of counties
706 showing absolute yield differences for maize, soybean, and wheat within 1 t ha$^{-1}$ compared to
707 observations. Differences between the two irrigation schemes are minimal: the irrig-unlim
708 scheme performs slightly better for maize and soybean in terms of average biases, while the
709 irrig-lim scheme shows better performance for wheat.

710 Furthermore, based on limited annual yield data, we observe that considering irrigation generally
711 improves the model's ability to capture inter-annual yield fluctuations (Figure S16). The KGE of
712 annual yields under the noirrig scheme are -1.342, -1.451, and -1.308 for maize, soybean, and
713 wheat, respectively, while with the irrig-umlim and irrig-lim schemes, the KGE values increase
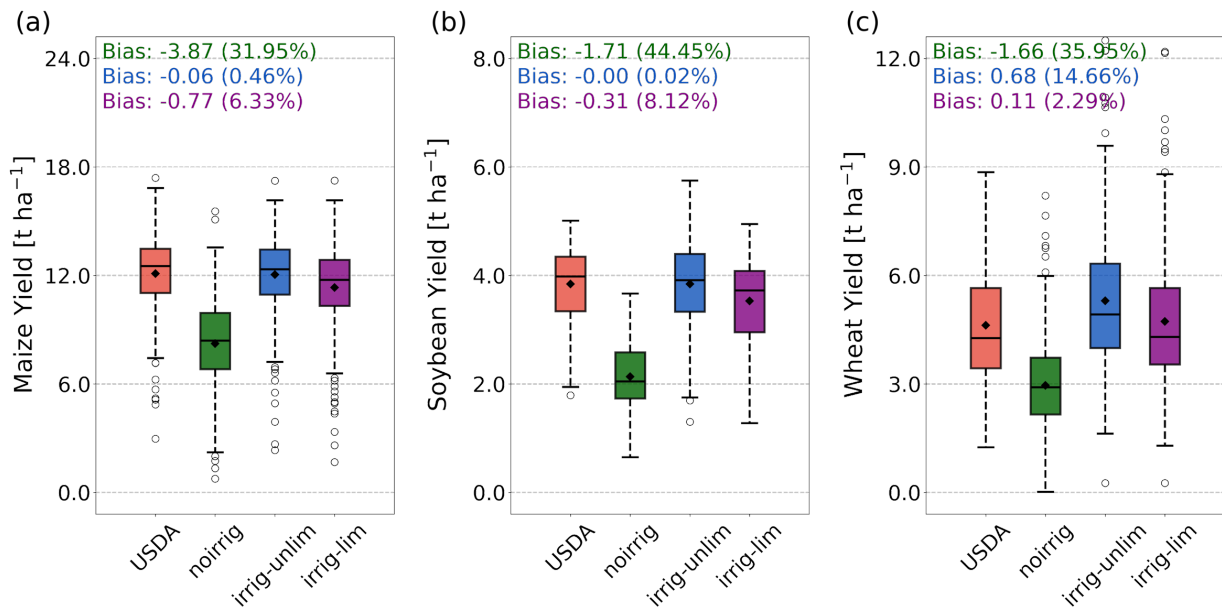714 to 0.101, -1.132, and 0.197, and -0.158, -1.449, and -0.144, respectively.

**Figure 10.** Evaluation of crop yield simulated using different schemes in the United States. (a) Maize yield in irrigated maize-growing regions of the United States, as reported by the USDA (orange boxes), compared with simulations by CoLM using the noirrig (green boxes), irrig-unlim (blue boxes), and irrig-lim (purple boxes) schemes. Since reported yields are at the county scale, grid-based simulation results were aggregated to corresponding counties. (b-c) Same as (a) but for soybean and wheat yields.

## 4. Discussions

### 4.1 Applications of the developed module

#### 4.1.1 Impacts of irrigation on energy budget

Numerous studies have highlighted the impacts of irrigation on global and regional energy budgets and near-surface climates. In this study, we similarly examine the effects of irrigation on the energy budget over irrigated areas in the U.S. by comparing results from the irrig-lim and noirrig scheme. Consistent with prior research, we find that irrigation increases latent heat (*LH*) by 7.53 W m$^{-2}$ (23.25 %) and decreases sensible heat (*SH*) by 5.18 W m$^{-2}$ (9.48 %) averaged from 2001 to 2016, resulting in an approximately 0.30°C reduction in land surface temperature (Figure 11). Since land-atmosphere coupling is not included, the primary mechanisms driving these impacts are increased soil evaporation due to enhanced soil moisture and greater vegetation transpiration driven by improved crop growth following irrigation (Figure S17 a-b). Annually, these mechanisms contribute roughly equally to the increase in total evapotranspiration in irrigated regions, with pronounced seasonal differences: during the peak growing seasons

737 (summer and autumn), the contribution was dominated by vegetation transpiration, while in other
738 seasons, particularly winter, the increase in soil evaporation plays a larger role in affecting
739 regional energy distribution and temperature (Figure S17c).

740 This study further explores the spatial characteristics of these impacts, analyzing the correlations
741 between irrigated area, irrigation water withdrawal, and changes in *LH*, *SH*, and land surface
742 temperature ($\Delta LH$, $\Delta SH$, $\Delta T_s$) across different climate zones. Notably, irrigation has the most
743 substantial impact in arid regions, especially on *LH*, where $\Delta LH$ is more than double that of
744 semi-arid and humid regions, with a larger reduction in temperature by 0.36°C. Interestingly,
745 while previous studies have emphasized irrigated area as the primary determinant of irrigation-
746 induced climate effects (Al-Yaari et al., 2022; Chen and Dirmeyer, 2019), our results indicate
747 that irrigation water withdrawal has a stronger influence on the regional energy budget and
748 temperature. Across all climate zones, $\Delta SH$, $\Delta LH$, and $\Delta T_s$ are significantly correlated ($p < 0.01$)
749 with irrigation water withdrawal, with correlation coefficients of -0.81, 0.79, and -0.82,
750 respectively (Figure 11 (b, e and h)), which are higher than the correlations with irrigated area (-
751 0.59, 0.61, and -0.52; Figure 11 (c, f and i)). This emphasizes the critical role of water
752 availability in modulating the climate effects of irrigation.

753 It is important to note that this study employs offline land simulations, which do not capture
754 land-atmosphere interactions, potentially introducing biases in the estimated climate impacts.
755 Previous studies have demonstrated that irrigation can induce both cooling and warming effects.
756 While increased evapotranspiration contributes to cooling, irrigation can also enhance
757 atmospheric water vapor content, leading to greater absorption of longwave radiation and
758 potential cloud formation, resulting in warming (Dessler and Sherwood, 2009; Hu et al., 2019).
759 These processes cannot be adequately represented in offline simulations, likely leading to an
760 overestimation of irrigation-induced cooling and a subsequent underestimation of temperature
761 (Figure 11g). Future studies should incorporate coupled land-atmosphere simulations to provide
762 a more comprehensive assessment (Cook et al., 2015; Puma and Cook, 2010; Sacks et al., 2009).
763 Another aspect worth considering is that some farmers irrigate not only to address water deficits
764 but also to mitigate heat stress during high-temperature periods (Verma et al., 2020). This
765 practice can notably affect local temperatures. For instance, surface water temperatures generally
766 track air temperatures, whereas groundwater temperatures remain relatively stable throughout the
767 year—typically warmer than air in winter and cooler in summer. This temperature difference,
768 especially in regions relying on groundwater irrigation, may have non-negligible effects on local
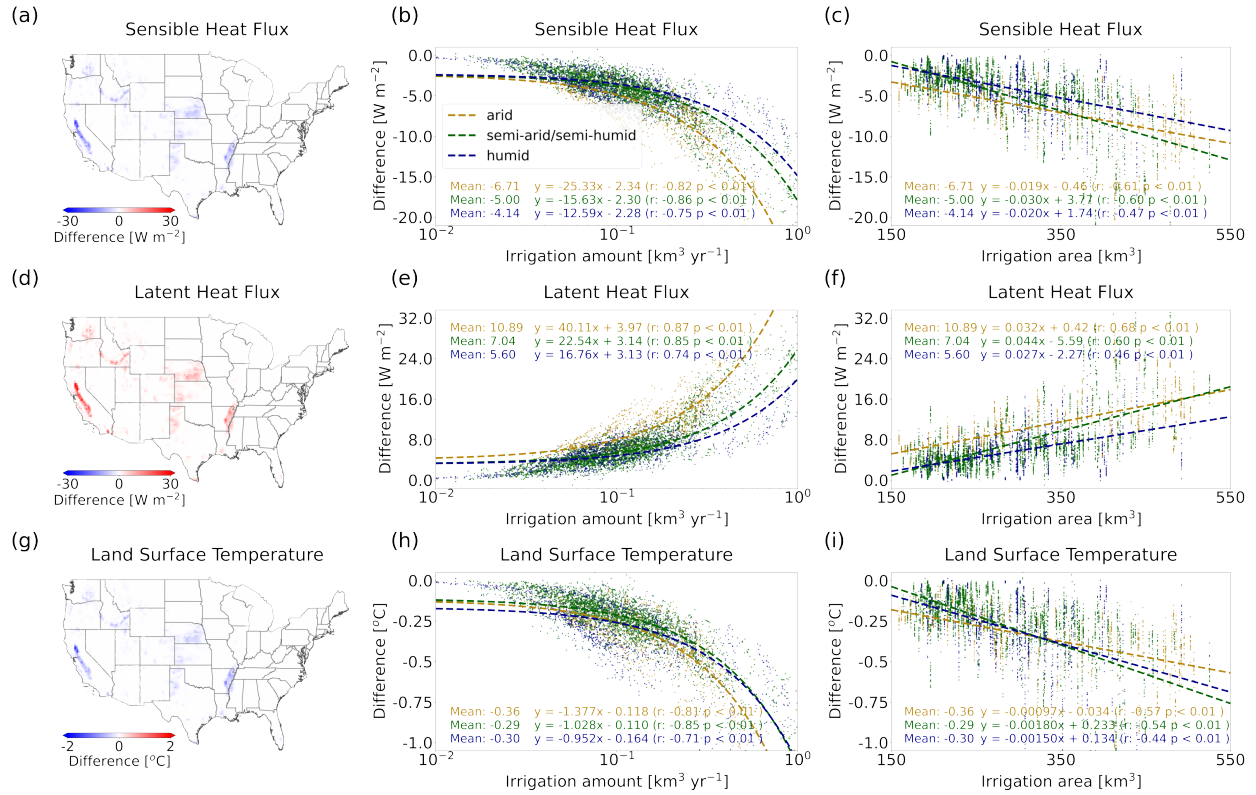769 climate that should be incorporated into future modeling efforts.

**Figure 11.** Impact of irrigation on local energy flux and surface temperature in the United States. (a) Impact of irrigation on sensible heat flux, quantified by the difference ($\Delta SH$) between the noirrig and irrig-lim simulation results. (b) Relationship between irrigation amount and $\Delta SH$, with grid colors indicating the climate zones (i.e., arid, semi-arid/semi-humid, humid). For each climate zone, the mean $\Delta SH$, the regression line of irrigation amount versus $\Delta SH$, and the regression equation are displayed. (c) Same as (b), but for the relationship between irrigation area and $\Delta SH$. (d-f) Same as (a-c), but for the impact on latent heat flux ($\Delta LH$). (g-i) Same as (a-c), but for the impact on land surface temperature ($\Delta T_s$).

### 4.1.2 Assessments of irrigation water security

This study compares the irrigation schemes with and without water availability constraints, highlighting the necessity and importance of incorporating water limitations into simulations. Our results demonstrate that including these constraints improves simulation accuracy, particularly in the modeling of water systems. Specifically, irrigation water withdrawal simulated under the irrig-lim scheme aligns more closely with observational data (Figure 3 and Figure 6). Validation against river flow observations further supports the improved performance of the irrig-lim scheme. Importantly, this scheme avoids the risk of potential water imbalances in the modeled hydrological system—an issue commonly associated with non-constrained schemes (Figure 8).

789 Additionally, incorporating water availability constraints more accurately reflects the reality of
790 water resource utilization. By accounting for the interconnections between subsystems within the
791 irrigation water demand-supply system, this approach enables simulation and prediction of
792 irrigation water security issues. Here, we visualize the average number of days when water
793 supply was insufficient to fully meet irrigation demand that simulated by the irrig-lim scheme
794 (Figure 12). Spatially, in humid regions, where irrigation demand is low and water resources are
795 abundant, fewer days of unmet irrigation needs occur. Conversely, in arid regions, where
796 irrigation demand is high and water resources are often limited, the number of unmet irrigation
797 days increases significantly. Figure 12a illustrates that states with a higher number of unmet
798 irrigation days are also those with relatively scarce water resources (e.g., Montana and Nevada).
799 From a temporal perspective, drought years lead to increased irrigation requirements due to
800 reduced precipitation or higher evaporative demand. Although additional water withdrawals can
801 partially address this increased demand, drought conditions often simultaneously result in
802 deficits in both surface and groundwater resources within the water system. As a result, most
803 states experience a substantial increase in unmet irrigation days during drought years (an average
804 of 43 days). In contrast, during wetter years, the number of unmet days decreases significantly
805 (an average of 31 days).

806 Reported disaster data show that even with irrigation, significant crop losses can occur during
807 drought years, aligning with broader water security challenges (Mieno et al., 2024). Our
808 approach effectively captures this phenomenon by describing the connectivity between
809 subsystems in the water demand-supply system and highlighting the impact of water limitations
810 on irrigation. In contrast, ignoring these constraints risks underestimating potential food security
811 issues in a future characterized by more frequent and/or severe droughts. This represents a
812 critical limitation of crop and land surface models that adopt irrigation schemes without
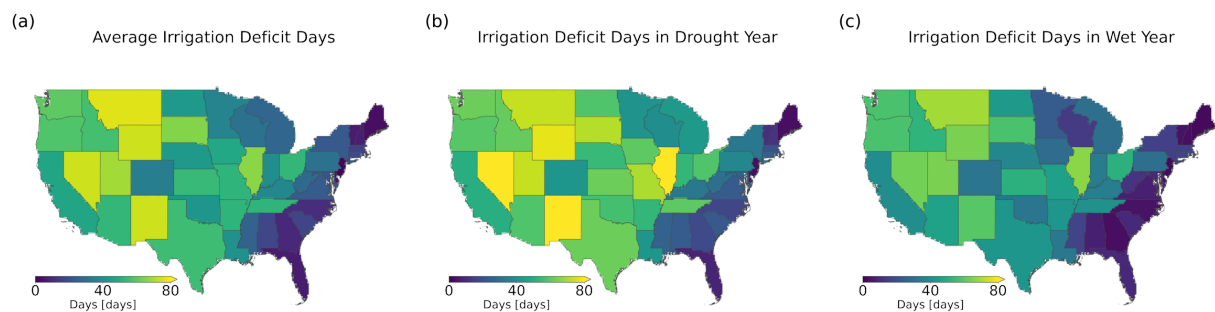813 considering water availability constraints.



814
815 **Figure 12.** Days per year with unmet irrigation demand (i.e., irrigation deficit days) in the United
816 States simulated by the irrig-lim scheme. (a) Multi-year average irrigation deficit days from 2001
817 to 2015 for individual states. (b) Irrigation deficit days in drought year for individual states. (c)
818 Irrigation deficit days in wet year for individual states. Drought year (wet year) is defined as the
819 year with the lowest (highest) annual precipitation during 2001–2016.

## 4.2 Limitations and a way forward

While the developed module represents a significant advancement in modeling irrigation water system within land surface models by providing a comprehensive representation of the irrigation processes—including water demand, water withdrawal, and water utilization, several limitations and assumptions should be acknowledged.

Irrigation water demand in this study is estimated using a soil moisture deficit method. However, the parameterization of certain key variables (e.g., target and threshold soil moisture levels) is overly simplified and does not account for variations among crop types. These parameters are adjustable, and their calibration could further enhance the model's accuracy in reproducing irrigation water use. Similarly, the fixed root depth of 1 m for all crops introduces additional uncertainty, potentially leading to overestimation or underestimation of irrigation demand. Incorporating dynamic root growth could better represent actual root zone depth based on crop-specific characteristics. Additionally, in some cases, farmers irrigate not only to address soil moisture deficits but also to reduce crop heat stress during high-temperature periods—a factor that should be incorporated into future modeling efforts. Furthermore, this study did not account for water losses during conveyance and application. Irrigation losses, as noted by Jägermeyr et al. (2015), include conveyance losses and on-field application losses. By ignoring conveyance losses, the model assumes that water withdrawn equals water applied, likely leading to an underestimation of total irrigation water use. Field application losses depend on irrigation methods (Leng et al., 2017), and while this study considered four irrigation systems with differentiated efficiencies, the reliance on simplified rules and a coarse irrigation map fails to reflect the diversity of irrigation methods and distributions. For example, actual sprinkler systems distribute water in specific spray patterns rather than uniformly. However, the model assumes uniform water distribution across each Crop Functional Type (CFT). Future models could benefit from parameterizations that capture spatial heterogeneity in irrigation distribution (Jägermeyr et al., 2015; Merriam et al., 1999). Moreover, irrigation water demand also depends on agricultural practices, such as crop types, cropping calendars, and planting intensities. While the model determines crop phenology based on meteorological data, real cropping calendars are influenced by farmers' decisions (Sacks et al., 2010). Incorporating satellite-derived phenology data could better represent these human factors. Addressing these agricultural practices is crucial for improving the accuracy and applicability of irrigation models.

In simulations of irrigation water withdrawal, this study provides a detailed representation of reservoir water withdrawal but acknowledges several sources of uncertainty: First, the dataset includes fewer dams than exist, as it focuses primarily on large dams and may lack data due to protection policies. This omission likely contributes to the underestimation of surface water extraction in some states. Second, all dams are assumed to supply irrigation water, although some reservoirs may not serve this purpose. The irrigation areas served by each dam are unknown, and a generalized estimation method is employed in this study, introducing large

858     uncertainties that remain difficult to validate. Third, dam operations are simplified, while in
859     reality, they often involve complex considerations, such as multi-objective operations and
860     coordinated management of multiple reservoirs. Advanced reservoir optimization strategies,
861     which require predictive simulations and prior knowledge of future inflows and demands, are not
862     incorporated into the model, presenting a significant challenge for considering the impacts of
863     complex human decision-making in land surface models.

864     Determining the division of irrigation water withdrawals between surface and groundwater
865     sources, as well as the withdrawal sequence, is also critical. This study allocates irrigation
866     demand based on pre-defined proportions and simultaneously withdraws water from both
867     sources. Surface water demand is met sequentially through local runoff, river discharge, and
868     upstream reservoir storages. This method, employed in models such as ORCHIDEE v2.2
869     (Arboleda-Obando et al., 2024) and E3SM (Zhou et al., 2020), provides satisfactory simulations
870     of water source allocation for irrigation (Figure 4 vs. Figure S19). However, its reliability
871     depends on the accuracy of input data and may underestimate withdrawals if any water source is
872     inadequately represented. Alternatively, some models (e.g., MATSIRO and CLM5; Pokhrel et al.,
873     2012; Yao et al., 2022) do not pre-allocate demand but set a fixed order of water withdrawals—
874     typically prioritizing surface water before groundwater. This method tends to satisfy more
875     irrigation demand and provides better estimates in regions with unreported groundwater
876     extraction. We propose that a hybrid approach, defining surface and groundwater proportions
877     dynamically, warrants consideration in future study. For instance, during wet seasons, surface
878     water extraction proportions could increase to reduce groundwater reliance and associated
879     pumping costs. Conversely, during dry seasons, surface water may be more constrained,
880     necessitating greater reliance on groundwater for irrigation. However, such an approach still
881     needs to address challenges, including unreported groundwater use, data scarcity, and the
882     physical, technical, and socio-economic constraints on groundwater use across regions.

883     Additionally, this study does not account for restrictions beyond water availability, such as local
884     regulations governing water allocation, including water rights and inter-basin water transfers.
885     Alternative water sources, such as desalinated seawater and treated wastewater, also warrant
886     consideration (Vliet et al., 2021). Recent assessments indicate that these unconventional water
887     sources are experiencing exponential growth (Jones et al., 2019). Although their contributions
888     remain low globally, they play a significant role in water-scarce regions. Incorporating these
889     factors into models could further improve simulations of irrigation water security.

890     The developed module's results and applicability are also strongly influenced by the CoLM
891     framework itself. A critical aspect requiring careful consideration is the evaluation and
892     calibration of hydrological variables, such as soil moisture, runoff, river discharge, and
893     groundwater levels, which are essential for water resource modeling. Currently, the CoLM
894     employs the simplified TOPMODEL (SIMTOP) developed by Niu et al. (2005) for runoff
895     simulations. The excessive simplification of this approach, coupled with the lack of calibration,
896     limits the model's accuracy in runoff simulations. Inadequate representation of snow and glacial

897  melt processes introduces regional biases, particularly in northern and midwestern U.S. states
898  where these factors are pivotal. For instance, surface water extraction is underestimated in some
899  states within these regions, likely because the model fails to accurately capture snowmelt and
900  glacial melt contributions to streamflow, leading to erroneous estimates of surface water
901  availability. Similarly, simulated evapotranspiration is systematically underestimated, even in
902  areas without crops or irrigation, likely due to more complex underlying causes. These biases,
903  when aggregated at the watershed level, result in significant discrepancies in river discharge,
904  thereby constraining the model's applicability for water resource management and its ability to
905  predict irrigation water security. Addressing these issues requires urgent improvements in the
906  representation of related processes, along with further calibration and parameter tuning.

907  Although the validation in this study is limited to the United States, the framework can be
908  applied to other regions with appropriate datasets. For example, the module requires defining the
909  allocation and sequence of withdrawals from surface water and groundwater sources. When
910  applying the model to other regions, the groundwater and surface water withdrawal ratios should
911  be pre-defined based on local infrastructure, such as groundwater extraction facilities, and the
912  withdrawal sequence can also be adjusted accordingly. For surface water withdrawals, it is
913  essential to prepare river network data and reservoir information for CaMa-Flood simulations.
914  Additionally, improving simulation accuracy may require incorporating region-specific crop
915  distribution (distinguishing rainfed and irrigated areas), crop characteristics (e.g., phenology,
916  photosynthetic capacity, carbon allocation), and management practices (e.g., planting dates,
917  irrigation strategies). Furthermore, CoLM offers multiple parameterization schemes for thermal,
918  hydrological, and biogeochemical processes, which should be evaluated for their suitability in
919  the target region.

## 5. Conclusions

921  The growing challenges posed by increasing global food demand and water scarcity underscore
922  the need for advanced modeling tools capable of accurately capturing human-water interactions.
923  This study contributes to addressing this need by implementing a two-way coupled irrigation
924  water system within the Common Land Model. The developed module provides a
925  comprehensive representation of the entire irrigation water use process, including water demand,
926  withdrawal, and utilization. It introduces a refined multi-source water withdrawal framework and
927  achieves bidirectional coupling between water demand and withdrawal during simulation.

928  The robustness of the new irrigation module is validated through simulations across the
929  contiguous United States, focusing on regional-scale water, energy, and crop yield dynamics. The
930  module effectively simulates total national annual irrigation withdrawals, their spatial
931  distribution, the proportions of different water sources, and irrigation volumes for various crops.
932  Compared to other hydrological models in ISIMIP2a, our model performs similarly or better in
933  simulating U.S. irrigation withdrawals. Incorporating the new irrigation module also
934  significantly improves the accuracy of simulated surface energy fluxes, both in magnitude and

31

935 seasonal patterns, resulting in more accurate surface temperature predictions. For streamflow, the
936 irrigation scheme accounting for water availability constraints enhances the model's
937 representation of hydrological system dynamics, whereas the unrestricted irrigation scheme
938 introduces potential water budget imbalances. Additionally, the new module markedly improves
939 the model's ability to simulate annual yields and interannual fluctuations of major crops,
940 including maize, soybean, and wheat.

941 We further apply the developed module in two novel analyses. First, the scheme effectively
942 characterizes the climatic impacts of irrigation, revealing a stronger positive correlation between
943 irrigation water volume, rather than irrigated area, and the intensity of irrigation-induced climatic
944 effects. This highlights the critical role of water availability in modulating irrigation-driven
945 climate impacts. Although more accurate simulation of these effects requires land-atmosphere
946 coupled modeling, the enhanced CoLM is clearly ready for such tasks. Second, the module
947 captures irrigation-related water security issues, particularly during drought years, where water
948 shortages across the resource system lead to irrigation water deficits and associated food security
949 challenges. These results demonstrate the promise of CoLM as a valuable tool for future water
950 use and scarcity assessments, paralleling the functionality of global hydrological models and
951 contributing to initiatives such as the Inter-Sectoral Impact Model Intercomparison Project.

952 **Data Availability Statement**

953 The meteorological variables from the WFDEI can be freely accessed from
954 ftp://rfdata:forceDATA@ftp.iiasa.ac.at. The land cover type datasets (MCD12Q1) can be freely
955 accessed from https://lpdaac.usgs.gov/products/mcd12q1v061/. The soil characteristics datasets
956 (GSDE) can be freely accessed from http://globalchange.bnu.edu.cn/research/data/. The
957 CropScape and Cropland Data Layer (CDL) datasets can be freely accessed from
958 https://nassgeodata.gmu.edu/CropScape/. The crop calendar datasets can be freely accessed from
959 https://zenodo.org/records/5062513/. The irrigation map and irrigation equipment percentage can
960 be freely accessed from https://www.fao.org/aquastat/en/geospatial-information/global-maps-
961 irrigated-areas/latest-version/. The GRanD database can be freely accessed from
962 https://www.globaldamwatch.org/grand/. The GRSAD database can be freely accessed from
963 https://dataverse.tdl.org/dataset.xhtml?persistentId=doi:10.18738/T8/DF80WG/. The ReGeom
964 database can be freely accessed from https://zenodo.org/records/1322884/. The USGS's
965 hydrological survey data can be freely accessed from https://water.usgs.gov/watuse/data/. The
966 USDA NASS's agricultural survey data can be freely accessed from
967 https://quickstats.nass.usda.gov/. The crop-specific irrigation water withdrawals data can be
968 freely accessed from https://doi.org/10.13012/B2IDB-2656127_V1/. The ISIMIP2a datasets can
969 be freely accessed from https://data.isimip.org/search/. The FluxCom datasets can be freely
970 accessed via ftp.bgc-jena.mpg.de. The ERA5-Land skin temperature data can be freely accessed
971 from https://cds.climate.copernicus.eu/datasets/reanalysis-era5-land-monthly-
972 means?tab=download/. The streamflow data (GRDC) can be freely accessed from

**Author contributions**

976 SZ and YD conceptualized and designed the study. SZ and HL collected the data, developed the
977 model, and conducted the analyses. FL and XL provided assistance with model development. HL
978 prepared the figures. SZ drafted the manuscript. All authors contributed to result interpretation
979 and reviewed the final manuscript.

**Competing interests**

981 The authors declare no competing interests.

**References**

992 Abdullah, K. bin: Use of water and land for food security and environmental sustainability,
993      Irrigation and Drainage, 55, 219–222, https://doi.org/10.1002/ird.254, 2006.
994 Al-Yaari, A., Ducharne, A., Thiery, W., Cheruy, F., and Lawrence, D.: The Role of Irrigation
995      Expansion on Historical Climate Change: Insights From CMIP6, Earth's Future, 10,
996      e2022EF002859, https://doi.org/10.1029/2022EF002859, 2022.
997 Arboleda-Obando, P. F., Ducharne, A., Yin, Z., and Ciais, P.: Validation of a new global irrigation
998      scheme in the land surface model ORCHIDEE v2.2, Geoscientific Model Development, 17,
999      2141–2164, https://doi.org/10.5194/gmd-17-2141-2024, 2024.
1000 Ball, J. T., Woodrow, I. E., and Berry, J. A.: A Model Predicting Stomatal Conductance and its
1001      Contribution to the Control of Photosynthesis under Different Environmental Conditions,
1002      in: Progress in Photosynthesis Research, edited by: Biggins, J., Springer, Dordrecht,
1003      Netherlands, 221–224, https://doi.org/10.1007/978-94-017-0519-6_48, 1987.
1004 Biemans, H., Haddeland, I., Kabat, P., Ludwig, F., Hutjes, R. W. A., Heinke, J., von Bloh, W.,
1005      and Gerten, D.: Impact of reservoirs on river discharge and irrigation water supply during

the 20th century, Water Resources Research, 47, https://doi.org/10.1029/2009WR008929, 2011.

Blyth, E. M., Arora, V. K., Clark, D. B., Dadson, S. J., De Kauwe, M. G., Lawrence, D. M., Melton, J. R., Pongratz, J., Turton, R. H., Yoshimura, K., and Yuan, H.: Advances in Land Surface Modelling, Current Climate Change Reports, 7, 45–71, https://doi.org/10.1007/s40641-021-00171-5, 2021.

Bonan, B.: A Land Surface Model (LSM Version 1.0) for Ecological, Hydrological, and Atmospheric Studies: Technical Description and User's Guide, University Corporation for Atmospheric Research, https://doi.org/10.5065/D6DF6P5X, 1996.

Buckingham, E. Studies on the Movement of Soil Moisture; US Department of Agriculture, Bureau of Soils: Washington, DC, USA, 1907.

Campbell, B., Beare, D., Bennett, E., Hall-Spencer, J., Ingram, J., Jaramillo, F., Ortiz, R., Ramankutty, N., Sayer, J., and Shindell, D.: Agriculture production as a major driver of the Earth system exceeding planetary boundaries, Ecology and Society, 22, https://doi.org/10.5751/ES-09595-220408, 2017.

Campbell, G. S.: A SIMPLE METHOD FOR DETERMINING UNSATURATED CONDUCTIVITY FROM MOISTURE RETENTION DATA, Soil Science, 117, 311, 1974.

Chen, L. and Dirmeyer, P. A.: Global observed and modelled impacts of irrigation on surface temperature, International Journal of Climatology, 39, 2587–2600, https://doi.org/10.1002/joc.5973, 2019.

Collatz, G. J., Ball, J. T., Grivet, C., and Berry, J. A.: Physiological and environmental regulation of stomatal conductance, photosynthesis and transpiration: a model that includes a laminar boundary layer, Agricultural and Forest Meteorology, 54, 107–136, https://doi.org/10.1016/0168-1923(91)90002-8, 1991.

Collatz, G. J., Ribas-Carbo, M., and Berry, J. A.: Coupled Photosynthesis-Stomatal Conductance Model for Leaves of C4 Plants, Functional Plant Biology, 19, 519–538, https://doi.org/10.1071/pp9920519, 1992.

Cook, B. I., Shukla, S. P., Puma, M. J., and Nazarenko, L. S.: Irrigation as an historical climate forcing, Climate Dynamics, 44, 1715–1730, https://doi.org/10.1007/s00382-014-2204-7, 2015.

Dai, Y., Dickinson, R. E., and Wang, Y.-P.: A Two-Big-Leaf Model for Canopy Temperature, Photosynthesis, and Stomatal Conductance, Journal of Climate, 17, 2281–2299, https://doi.org/10.1175/1520-0442(2004)017<2281:ATMFCT>2.0.CO;2, 2004.

Dai, Y., Xin, Q., Wei, N., Zhang, Y., Shangguan, W., Yuan, H., Zhang, S., Liu, S., and Lu, X.: A Global High-Resolution Data Set of Soil Hydraulic and Thermal Properties for Land Surface Modeling, Journal of Advances in Modeling Earth Systems, 11, 2996–3023, https://doi.org/10.1029/2019MS001784, 2019.

Dai, Y. and Yuan, H.: CoLM2014 [code], https://github.com/Hi-Res-CoLM/CoLM2014, 2014

Dai, Y. and Zeng, Q.: A land surface model (IAP94) for climate studies part I: Formulation and validation in off-line experiments, Advances in Atmospheric Sciences, 14, 433–460, https://doi.org/10.1007/s00376-997-0063-4, 1997.

Dai, Y., Zeng, X., Dickinson, R. E., Baker, I., Bonan, G. B., Bosilovich, M. G., Denning, A. S., Dirmeyer, P. A., Houser, P. R., Niu, G., Oleson, K. W., Schlosser, C. A., and Yang, Z.-L.: The Common Land Model, Bulletin of the American Meteorological Society, 84, 1013–1024, https://doi.org/10.1175/BAMS-84-8-1013, 2003.

Dessler, A. E. and Sherwood, S. C.: A Matter of Humidity, Science, 323, 1020–1021, https://doi.org/10.1126/science.1171264, 2009.

Dickinson, E., Henderson-Sellers, A., and Kennedy, J.: Biosphere-atmosphere Transfer Scheme (BATS) Version 1e as Coupled to the NCAR Community Climate Model, University Corporation for Atmospheric Research, https://doi.org/10.5065/D67W6959, 1993.

Dieter, C. A., Maupin, M. A., Caldwell, R. R., Harris, M. A., Ivahnenko, T. I., Lovelace, J. K., Barber, N. L., and Linsey, K. S.: Estimated use of water in the United States in 2015, Circular, U.S. Geological Survey, https://doi.org/10.3133/cir1441, 2018.

Döll, P., Müller Schmied, H., Schuh, C., Portmann, F. T., and Eicker, A.: Global-scale assessment of groundwater depletion and related groundwater abstractions: Combining hydrological modeling with information from well observations and GRACE satellites, Water Resources Research, 50, 5698–5720, https://doi.org/10.1002/2014WR015595, 2014.

Döll, P., Trautmann, T., Gerten, D., Schmied, H. M., Ostberg, S., Saaed, F., and Schleussner, C.-F.: Risks for the global freshwater system at 1.5 °C and 2 °C global warming, Environmental Research Letters, 13, 044038, https://doi.org/10.1088/1748-9326/aab792, 2018.

Douglas, E. M., Beltrán-Przekurat, A., Niyogi, D., Pielke, R. A., and Vörösmarty, C. J.: The impact of agricultural intensification and irrigation on land–atmosphere interactions and Indian monsoon precipitation — A mesoscale modeling perspective, Global and Planetary Change, 67, 117–128, https://doi.org/10.1016/j.gloplacha.2008.12.007, 2009.

Drewniak, B., Song, J., Prell, J., Kotamarthi, V. R., and Jacob, R.: Modeling agriculture in the Community Land Model, Geoscientific Model Development, 6, 495–515, https://doi.org/10.5194/gmd-6-495-2013, 2013.

Druel, A., Munier, S., Mucia, A., Albergel, C., and Calvet, J.-C.: Implementation of a new crop phenology and irrigation scheme in the ISBA land surface model using SURFEX_v8.1, Geoscientific Model Development, 15, 8453–8471, https://doi.org/10.5194/gmd-15-8453-2022, 2022.

Farquhar, G. D., von Caemmerer, S., and Berry, J. A.: A biochemical model of photosynthetic $CO_2$ assimilation in leaves of C3 species, Planta, 149, 78–90, https://doi.org/10.1007/BF00386231, 1980.

Friedl, M., Sulla-Menashe, D.: MODIS/Terra+Aqua Land Cover Type Yearly L3 Global 500m SIN Grid V061. NASA EOSDIS Land Processes Distributed Active Archive Center [data set], https://doi.org/10.5067/MODIS/MCD12Q1.061, 2022

1084   Gosling, S., Müller Schmied, H., Betts, R., Chang, J., Ciais, P., Dankers, R., Döll, P., Eisner, S.,
1085        Flörke, M., Gerten, D., Grillakis, M., Hanasaki, N., Hagemann, S., Huang, M., Huang, Z.,
1086        Jerez, S., Kim, H., Koutroulis, A., Leng, G., Liu, X., Masaki, Y., Montavez, P.,
1087        Morfopoulos, C., Oki, T., Papadimitriou, L., Pokhrel, Y., Portmann, F. T., Orth, R., Ostberg,
1088        S., Satoh, Y., Seneviratne, S., Sommer, P., Stacke, T., Tang, Q., Tsanis, I., Wada, Y., Zhou,
1089        T., Büchner, M., Schewe, J., and Zhao, F.: ISIMIP2a Simulation Data from Water (global)
1090        Sector (V. 1.1), in, GFZ Data Services, https://doi.org/10.5880/PIK.2019.003, 2019.

1091   GRDC: The Global Runoff Database, Global Runoff Data Centre [data set],
1092        https://www.bafg.de/GRDC/EN/Home/, 2023

1093   Hanasaki, N., Yoshikawa, S., Pokhrel, Y., and Kanae, S.: A global hydrological simulation to
1094        specify the sources of water used by humans, Hydrology and Earth System Sciences, 22,
1095        789–817, https://doi.org/10.5194/hess-22-789-2018, 2018.

1096   Hanazaki, R., Yamazaki, D., and Yoshimura, K.: Development of a Reservoir Flood Control
1097        Scheme for Global Flood Models, Journal of Advances in Modeling Earth Systems, 14,
1098        e2021MS002944, https://doi.org/10.1029/2021MS002944, 2022.

1099   Hu, Z., Xu, Z., Ma, Z., Mahmood, R., and Yang, Z.: Potential surface hydrologic responses to
1100        increases in greenhouse gas concentrations and land use and land cover changes,
1101        International Journal of Climatology, 39, 814–827, https://doi.org/10.1002/joc.5844, 2019.

1102   Jägermeyr, J., Gerten, D., Heinke, J., Schaphoff, S., Kummu, M., and Lucht, W.: Water savings
1103        potentials of irrigation systems: global simulation of processes and linkages, Hydrology and
1104        Earth System Sciences, 19, 3073–3091, https://doi.org/10.5194/hess-19-3073-2015, 2015.

1105   Jägermeyr, J., Müller, C., Ruane, A. C., Elliott, J., Balkovic, J., Castillo, O., Faye, B., Foster, I.,
1106        Folberth, C., and Franke, J. A.: Climate impacts on global agriculture emerge earlier in new
1107        generation of climate and crop models, Nature Food, 2, 873–885,
1108        https://doi.org/10.1038/s43016-021-00400-y, 2021.

1109   Jasechko, S., Seybold, H., Perrone, D., Fan, Y., Shamsudduha, M., Taylor, R. G., Fallatah, O.,
1110        and Kirchner, J. W.: Rapid groundwater decline and some cases of recovery in aquifers
1111        globally, Nature, 625, 715–721, https://doi.org/10.1038/s41586-023-06879-8, 2024.

1112   Jung, M., Koirala, S., Weber, U., Ichii, K., Gans, F., Camps-Valls, G., Papale, D., Schwalm, C.,
1113        Tramontana, G., and Reichstein, M.: The FLUXCOM ensemble of global land-atmosphere
1114        energy fluxes, Scientific Data, 6, 74, https://doi.org/10.1038/s41597-019-0076-8, 2019.

1115   Kang, S. and Eltahir, E. A. B.: North China Plain threatened by deadly heatwaves due to climate
1116        change and irrigation, Nature Communications, 9, 2894, https://doi.org/10.1038/s41467-
1117        018-05252-y, 2018.

1118   Ketchum, D., Hoylman, Z. H., Huntington, J., Brinkerhoff, D., and Jencso, K. G.: Irrigation
1119        intensification impacts sustainability of streamflow in the Western United States,
1120        Communications Earth & Environment, 4, 1–8, https://doi.org/10.1038/s43247-023-01152-
1121        2, 2023.

1122   Lehner, B., Liermann, C. R., Revenga, C., Vörösmarty, C., Fekete, B., Crouzet, P., Döll, P.,
1123        Endejan, M., Frenken, K., Magome, J., Nilsson, C., Robertson, J. C., Rödel, R., Sindorf, N.,

and Wisser, D.: High-resolution mapping of the world's reservoirs and dams for sustainable river-flow management, Frontiers in Ecology and the Environment, 9, 494–502, https://doi.org/10.1890/100125, 2011.

Leng, G., Huang, M., Tang, Q., and Leung, L. R.: A modeling study of irrigation effects on global surface water and groundwater resources under a changing climate, Journal of Advances in Modeling Earth Systems, 7, 1285–1304, https://doi.org/10.1002/2015MS000437, 2015.

Leng, G., Leung, L. R., and Huang, M.: Significant impacts of irrigation water sources and methods on modeling irrigation effects in the ACME Land Model, Journal of Advances in Modeling Earth Systems, 9, 1665–1683, https://doi.org/10.1002/2016MS000885, 2017.

Li, C., Lu, H., Yang, K., Wright, J. S., Yu, L., Chen, Y., Huang, X., and Xu, S.: Evaluation of the Common Land Model (CoLM) from the Perspective of Water and Energy Budget Simulation: Towards Inclusion in CMIP6, Atmosphere, 8, 141, https://doi.org/10.3390/atmos8080141, 2017a.

Li, C., Yuan, X., Jiao, Y., Ji, P., and Huang, Z.: High-resolution land surface modeling of the irrigation effects on evapotranspiration over the Yellow River basin, Journal of Hydrology, 633, 130986, https://doi.org/10.1016/j.jhydrol.2024.130986, 2024a.

Li, D., Wrzesien, M. L., Durand, M., Adam, J., and Lettenmaier, D. P.: How much runoff originates as snow in the western United States, and how will that change in the future?, Geophysical Research Letters, 44, 6163–6172, https://doi.org/10.1002/2017GL073551, 2017b.

Li, F., Zhou, Z., Levis, S., Sitch, S., Hayes, F., Feng, Z., Reich, P. B., Zhao, Z., and Zhou, Y.: Quantifying the role of ozone-caused damage to vegetation in the Earth system: a new parameterization scheme for photosynthetic and stomatal responses, Geoscientific Model Development, 17, 6173–6193, https://doi.org/10.5194/gmd-17-6173-2024, 2024b.

Li, H., Huang, M., Wigmosta, M. S., Ke, Y., Coleman, A. M., Leung, L. R., Wang, A., and Ricciuto, D. M.: Evaluating runoff simulations from the Community Land Model 4.0 using observations from flux towers and a mountainous watershed, Journal of Geophysical Research: Atmospheres, 116, https://doi.org/10.1029/2011JD016276, 2011.

Li, H., Lo, M.-H., Ryu, D., Peel, M., and Zhang, Y.: Possible Increase of Air Temperature by Irrigation, Geophysical Research Letters, 49, e2022GL100427, https://doi.org/10.1029/2022GL100427, 2022.

Liang, X., Lettenmaier, D. P., Wood, E. F., and Burges, S. J.: A simple hydrologically based model of land surface water and energy fluxes for general circulation models, Journal of Geophysical Research: Atmospheres, 99, 14415–14428, https://doi.org/10.1029/94JD00483, 1994.

Liu, S., Zeng, X., Dai, Y., Yuan, H., Wei, N., Wei, Z., Lu, X., and Zhang, S.: A Surface Flux Estimation Scheme Accounting for Large-Eddy Effects for Land Surface Modeling, Geophysical Research Letters, 49, e2022GL101754, https://doi.org/10.1029/2022GL101754, 2022.

Lombardozzi, D. L., Lu, Y., Lawrence, P. J., Lawrence, D. M., Swenson, S., Oleson, K. W., Wieder, W. R., and Ainsworth, E. A.: Simulating Agriculture in the Community Land Model Version 5, Journal of Geophysical Research: Biogeosciences, 125, e2019JG005529, https://doi.org/10.1029/2019JG005529, 2020.

Lu, Y., Jin, J., and Kueppers, L. M.: Crop growth and irrigation interact to influence surface fluxes in a regional climate-cropland model (WRF3.3-CLM4crop), Climate Dynamics, 45, 3347–3363, https://doi.org/10.1007/s00382-015-2543-z, 2015.

Malek, K., Stöckle, C., Chinnayakanahalli, K., Nelson, R., Liu, M., Rajagopalan, K., Barik, M., and Adam, J. C.: VIC–CropSyst-v2: A regional-scale modeling platform to simulate the nexus of climate, hydrology, cropping systems, and human decisions, Geoscientific Model Development, 10, 3059–3084, https://doi.org/10.5194/gmd-10-3059-2017, 2017.

McDermid, S., Nocco, M., Lawston-Parker, P., Keune, J., Pokhrel, Y., Jain, M., Jägermeyr, J., Brocca, L., Massari, C., Jones, A. D., Vahmani, P., Thiery, W., Yao, Y., Bell, A., Chen, L., Dorigo, W., Hanasaki, N., Jasechko, S., Lo, M.-H., Mahmood, R., Mishra, V., Mueller, N. D., Niyogi, D., Rabin, S. S., Sloat, L., Wada, Y., Zappa, L., Chen, F., Cook, B. I., Kim, H., Lombardozzi, D., Polcher, J., Ryu, D., Santanello, J., Satoh, Y., Seneviratne, S., Singh, D., and Yokohata, T.: Irrigation in the Earth system, Nature Reviews Earth & Environment, 1–19, https://doi.org/10.1038/s43017-023-00438-5, 2023.

McDermid, S. S., Mearns, L. O., and Ruane, A. C.: Representing agriculture in Earth System Models: Approaches and priorities for development, Journal of Advances in Modeling Earth Systems, 9, 2230–2265, https://doi.org/10.1002/2016MS000749, 2017.

Mehta, P., Siebert, S., Kummu, M., Deng, Q., Ali, T., Marston, L., Xie, W., and Davis, K. F.: Half of twenty-first century global irrigation expansion has been in water-stressed regions, Nature Water, 2, 254–261, https://doi.org/10.1038/s44221-024-00206-9, 2024.

Merriam, J. L., Burt, C. M., Clemmens, A. J., Solomon, K. H., Howell, T. A., and Strelkoff, T. S.: Irrigation Performance Measures: Efficiency and Uniformity, Journal of Irrigation and Drainage Engineering, 125, 97–99, https://doi.org/10.1061/(ASCE)0733-9437(1999)125:2(97), 1999.

Mieno, T., Foster, T., Kakimoto, S., and Brozović, N.: Aquifer depletion exacerbates agricultural drought losses in the US High Plains, Nature Water, 2, 41–51, https://doi.org/10.1038/s44221-023-00173-7, 2024.

Müller Schmied, H., Cáceres, D., Eisner, S., Flörke, M., Herbert, C., Niemann, C., Peiris, T. A., Popat, E., Portmann, F. T., Reinecke, R., Schumacher, M., Shadkam, S., Telteu, C.-E., Trautmann, T., and Döll, P.: The global water resources and use model WaterGAP v2.2d: model description and evaluation, Geoscientific Model Development, 14, 1037–1079, https://doi.org/10.5194/gmd-14-1037-2021, 2021.

Muñoz-Sabater, J., Dutra, E., Agustí-Panareda, A., Albergel, C., Arduini, G., Balsamo, G., Boussetta, S., Choulga, M., Harrigan, S., Hersbach, H., Martens, B., Miralles, D. G., Piles, M., Rodríguez-Fernández, N. J., Zsoter, E., Buontempo, C., and Thépaut, J.-N.: ERA5-

Land: a state-of-the-art global reanalysis dataset for land applications, Earth System Science Data, 13, 4349–4383, https://doi.org/10.5194/essd-13-4349-2021, 2021.

Nair, S., Johnson, J., and Wang, C.: Efficiency of Irrigation Water Use: A Review from the Perspectives of Multiple Disciplines, Agronomy Journal, 105, 351–363, https://doi.org/10.2134/agronj2012.0421, 2013.

Nazemi, A. and Wheater, H. S.: On inclusion of water resource management in Earth system models &ndash; Part 1: Problem definition and representation of water demand, Hydrology and Earth System Sciences, 19, 33–61, https://doi.org/10.5194/hess-19-33-2015, 2015.

Niu, G.-Y., Yang, Z.-L., Dickinson, R. E., and Gulden, L. E.: A simple TOPMODEL-based runoff parameterization (SIMTOP) for use in global climate models, Journal of Geophysical Research: Atmospheres, 110, https://doi.org/10.1029/2005JD006111, 2005.

Nocco, M. A., Smail, R. A., and Kucharik, C. J.: Observation of irrigation-induced climate change in the Midwest United States, Global Change Biology, 25, 3472–3484, https://doi.org/10.1111/gcb.14725, 2019.

Ozdogan, M., Rodell, M., Beaudoing, H. K., and Toll, D. L.: Simulating the Effects of Irrigation over the United States in a Land Surface Model Based on Satellite-Derived Agricultural Data, Journal of Hydrometeorology, 11, 171–184, https://doi.org/10.1175/2009JHM1116.1, 2010.

Pekel, J.-F., Cottam, A., Gorelick, N., and Belward, A. S.: High-resolution mapping of global surface water and its long-term changes, Nature, 540, 418–422, https://doi.org/10.1038/nature20584, 2016.

Phillips, C. E., Nair, U. S., Mahmood, R., Rappin, E., and Pielke, R. A.: Influence of Irrigation on Diurnal Mesoscale Circulations: Results From GRAINEX, Geophysical Research Letters, 49, e2021GL096822, https://doi.org/10.1029/2021GL096822, 2022.

Pokhrel, Y., Hanasaki, N., Koirala, S., Cho, J., Yeh, P. J.-F., Kim, H., Kanae, S., and Oki, T.: Incorporating Anthropogenic Water Regulation Modules into a Land Surface Model, Journal of Hydrometeorology, 13, 255–269, https://doi.org/10.1175/JHM-D-11-013.1, 2012.

Pokhrel, Y. N., Hanasaki, N., Wada, Y., and Kim, H.: Recent progresses in incorporating human land–water management into global land surface models toward their integration into Earth system models, WIREs Water, 3, 548–574, https://doi.org/10.1002/wat2.1150, 2016.

Puma, M. J. and Cook, B. I.: Effects of irrigation on global climate during the 20th century, Journal of Geophysical Research: Atmospheres, 115, https://doi.org/10.1029/2010JD014122, 2010.

Rappin, E. D., Mahmood, R., Nair, U. S., and Sr, R. A. P.: Land–Atmosphere Interactions during GRAINEX: Planetary Boundary Layer Evolution in the Presence of Irrigation, Journal of Hydrometeorology, 23, 1401–1417, https://doi.org/10.1175/JHM-D-21-0160.1, 2022.

Richards, L. A.: CAPILLARY CONDUCTION OF LIQUIDS THROUGH POROUS MEDIUMS, Physics, 1, 318–333, https://doi.org/10.1063/1.1745010, 1931.

Rodell, M. and Reager, J. T.: Water cycle science enabled by the GRACE and GRACE-FO satellite missions, Nat Water, 1, 47–59, https://doi.org/10.1038/s44221-022-00005-0, 2023.

Ruess, P. J., Konar, M., Wanders, N., and Bierkens, M. F. P.: Total irrigation by crop in the Continental United States from 2008 to 2020, Scientific Data, 11, 395, https://doi.org/10.1038/s41597-024-03244-w, 2024.

Russo, T. A. and Lall, U.: Depletion and response of deep groundwater to climate-induced pumping variability, Nature Geoscience, 10, 105–108, https://doi.org/10.1038/ngeo2883, 2017.

Sacks, W. J., Cook, B. I., Buenning, N., Levis, S., and Helkowski, J. H.: Effects of global irrigation on the near-surface climate, Climate Dynamics, 33, 159–175, https://doi.org/10.1007/s00382-008-0445-z, 2009.

Sacks, W. J., Deryng, D., Foley, J. A., and Ramankutty, N.: Crop planting dates: an analysis of global patterns, Global Ecology and Biogeography, 19, 607–620, https://doi.org/10.1111/j.1466-8238.2010.00551.x, 2010.

Schewe, J., Heinke, J., Gerten, D., Haddeland, I., Arnell, N. W., Clark, D. B., Dankers, R., Eisner, S., Fekete, B. M., Colón-González, F. J., Gosling, S. N., Kim, H., Liu, X., Masaki, Y., Portmann, F. T., Satoh, Y., Stacke, T., Tang, Q., Wada, Y., Wisser, D., Albrecht, T., Frieler, K., Piontek, F., Warszawski, L., and Kabat, P.: Multimodel assessment of water scarcity under climate change, Proceedings of the National Academy of Sciences, 111, 3245–3250, https://doi.org/10.1073/pnas.1222460110, 2014.

Schlosser, C. A., Strzepek, K., Gao, X., Fant, C., Blanc, É., Paltsev, S., Jacoby, H., Reilly, J., and Gueneau, A.: The future of global water stress: An integrated assessment, Earth's Future, 2, 341–361, https://doi.org/10.1002/2014EF000238, 2014.

Sellers, P. J., Randall, D. A., Collatz, G. J., Berry, J. A., Field, C. B., Dazlich, D. A., Zhang, C., Collelo, G. D., and Bounoua, L.: A Revised Land Surface Parameterization (SiB2) for Atmospheric GCMS. Part I: Model Formulation, Journal of Climate, 9, 676–705, https://doi.org/10.1175/1520-0442(1996)009<0676:ARLSPF>2.0.CO;2, 1996.

Shangguan, W., Dai, Y., Duan, Q., Liu, B., and Yuan, H.: A global soil data set for earth system modeling, Journal of Advances in Modeling Earth Systems, 6, 249–263, https://doi.org/10.1002/2013MS000293, 2014.

Shen, X., Chen, Q., Sun, J., Huang, W., Gong, J., Li, Z., and Wang, J.: Development of Operational Global Medium-Range Forecast System in National Meteorological Centre, Meteorological Monthly, 47, 645–654, https://doi.org/10.7519/j.issn.1000-0526.2021.06.001, 2021.

Siebert, S. and Döll, P.: Quantifying blue and green virtual water contents in global crop production as well as potential production losses without irrigation, Journal of Hydrology, 384, 198–217, https://doi.org/10.1016/j.jhydrol.2009.07.031, 2010.

Siebert, S., Burke, J., Faures, J. M., Frenken, K., Hoogeveen, J., Döll, P., and Portmann, F. T.: Groundwater use for irrigation – a global inventory, Hydrology and Earth System Sciences, 14, 1863–1880, https://doi.org/10.5194/hess-14-1863-2010, 2010.

Siebert, S., Henrich, V., Frenken, K., and Burke, J.: Update of The Digital Global Map Of Irrigation Areas to Version 5, Rheinische Friedrich-Wilhelms-University, Bonn, Germany/Food and Agriculture Organization of the United Nations, Rome, Italy, 2013.

Sood, A. and Smakhtin, V.: Global hydrological models: a review, Hydrological Sciences Journal, 60, 549–565, https://doi.org/10.1080/02626667.2014.950580, 2015.

Sutanudjaja, E. H., van Beek, R., Wanders, N., Wada, Y., Bosmans, J. H. C., Drost, N., van der Ent, R. J., de Graaf, I. E. M., Hoch, J. M., de Jong, K., Karssenberg, D., López López, P., Peßenteiner, S., Schmitz, O., Straatsma, M. W., Vannametee, E., Wisser, D., and Bierkens, M. F. P.: PCR-GLOBWB 2: a 5 arcmin global hydrological and water resources model, Geoscientific Model Development, 11, 2429–2453, https://doi.org/10.5194/gmd-11-2429-2018, 2018.

Tang, Q., Oki, T., Kanae, S., and Hu, H.: The Influence of Precipitation Variability and Partial Irrigation within Grid Cells on a Hydrological Simulation, Journal of Hydrometeorology, 8, 499–512, https://doi.org/10.1175/JHM589.1, 2007.

Taranu, S. I., Lawrence, D. M., Wada, Y., Tang, T., Kluzek, E., Rabin, S., Yao, Y., De Hertog, S. J., Vanderkelen, I., and Thiery, W.: Bridging the gap: a new module for human water use in the Community Earth System Model version 2.2.1, Geoscientific Model Development, 17, 7365–7399, https://doi.org/10.5194/gmd-17-7365-2024, 2024.

Thiery, W., Davin, E. L., Lawrence, D. M., Hirsch, A. L., Hauser, M., and Seneviratne, S. I.: Present-day irrigation mitigates heat extremes, Journal of Geophysical Research: Atmospheres, 122, 1403–1422, https://doi.org/10.1002/2016JD025740, 2017.

USDA: National Agricultural Statistics Service Cropland Data Layer, Published crop-specific data layer, Washington, DC [data set], https://nassgeodata.gmu.edu/CropScape USDA-NASS, 2019.

USDA/NASS: Census of Agriculture, USDA - National Agricultural Statistics Service [data set], https://quickstats.nass.usda.gov/, 2023.

USGS: Water Use in the United States, USGS Water Data for the Nation [data set], https://water.usgs.gov/watuse/data/, 2023

Verma, S., Kumar, N., Verma, A., Singh, H., Siddique, K. H. M., and Singh, N. P.: Novel approaches to mitigate heat stress impacts on crop growth and development, Plant Physiology Reports, 25, 627–644, https://doi.org/10.1007/s40502-020-00550-4, 2020.

Vliet, M. T. H. van, Jones, E. R., Flörke, M., Franssen, W. H. P., Hanasaki, N., Wada, Y., and Yearsley, J. R.: Global water scarcity including surface water quality and expansions of clean water technologies, Environmental Research Letters, 16, 024020, https://doi.org/10.1088/1748-9326/abbfc3, 2021.

de Vrese, P., Hagemann, S., and Claussen, M.: Asian irrigation, African rain: Remote impacts of irrigation, Geophysical Research Letters, 43, 3737–3745, https://doi.org/10.1002/2016GL068146, 2016.

de Vrese, P., Stacke, T., and Hagemann, S.: Exploring the biogeophysical limits of global food production under different climate change scenarios, Earth System Dynamics, 9, 393–412, https://doi.org/10.5194/esd-9-393-2018, 2018.

Watkins, M. M., Wiese, D. N., Yuan, D.-N., Boening, C., and Landerer, F. W.: Improved methods for observing Earth's time variable mass distribution with GRACE using spherical cap mascons, Journal of Geophysical Research: Solid Earth, 120, 2648–2671, https://doi.org/10.1002/2014JB011547, 2015.

Weedon, G. P., Balsamo, G., Bellouin, N., Gomes, S., Best, M. J., and Viterbo, P.: The WFDEI meteorological forcing data set: WATCH Forcing Data methodology applied to ERA-Interim reanalysis data, Water Resources Research, 50, 7505–7514, https://doi.org/10.1002/2014WR015638, 2014.

Wiese, D. N., Landerer, F. W., and Watkins, M. M.: Quantifying and reducing leakage errors in the JPL RL05M GRACE mascon solution, Water Resources Research, 52, 7490–7502, https://doi.org/10.1002/2016WR019344, 2016.

Wisser, D., Fekete, B. M., Vörösmarty, C. J., and Schumann, A. H.: Reconstructing 20th century global hydrography: a contribution to the Global Terrestrial Network- Hydrology (GTN-H), Hydrology and Earth System Sciences, 14, 1–24, https://doi.org/10.5194/hess-14-1-2010, 2010.

Yamazaki, D., Kanae, S., Kim, H., and Oki, T.: A physically based description of floodplain inundation dynamics in a global river routing model, Water Resources Research, 47, https://doi.org/10.1029/2010WR009726, 2011.

Yamazaki, D., Ikeshima, D., Sosa, J., Bates, P. D., Allen, G. H., and Pavelsky, T. M.: MERIT Hydro: A High-Resolution Global Hydrography Map Based on Latest Topography Dataset, Water Resources Research, 55, 5053–5073, https://doi.org/10.1029/2019WR024873, 2019.

Yang, Y., Jin, Z., Mueller, N. D., Driscoll, A. W., Hernandez, R. R., Grodsky, S. M., Sloat, L. L., Chester, M. V., Zhu, Y.-G., and Lobell, D. B.: Sustainable irrigation and climate feedbacks, Nature Food, 4, 654–663, https://doi.org/10.1038/s43016-023-00821-x, 2023.

Yao, Y., Vanderkelen, I., Lombardozzi, D., Swenson, S., Lawrence, D., Jägermeyr, J., Grant, L., and Thiery, W.: Implementation and Evaluation of Irrigation Techniques in the Community Land Model, Journal of Advances in Modeling Earth Systems, 14, e2022MS003074, https://doi.org/10.1029/2022MS003074, 2022.

Yigzaw, W., Li, H.-Y., Demissie, Y., Hejazi, M. I., Leung, L. R., Voisin, N., and Payn, R.: A New Global Storage-Area-Depth Data Set for Modeling Reservoirs in Land Surface and Earth System Models, Water Resources Research, 54, 10,372-10,386, https://doi.org/10.1029/2017WR022040, 2018.

Yuan, H., Dai, Y., Dickinson, R. E., Pinty, B., Shangguan, W., Zhang, S., Wang, L., and Zhu, S.: Reexamination and further development of two-stream canopy radiative transfer models for global land modeling, Journal of Advances in Modeling Earth Systems, 9, 113–129, https://doi.org/10.1002/2016MS000773, 2017.

1358  Yuan, X. and Liang, X.-Z.: Evaluation of a Conjunctive Surface–Subsurface Process Model
1359      (CSSP) over the Contiguous United States at Regional–Local Scales, Journal of
1360      Hydrometeorology, 12, 579–599, https://doi.org/10.1175/2010JHM1302.1, 2011.
1361  Zeng, X. and Dickinson, R. E.: Effect of Surface Sublayer on Surface Skin Temperature and
1362      Fluxes, Journal of Climate, 11, 537–550, https://doi.org/10.1175/1520-
1363      0442(1998)011<0537:EOSSOS>2.0.CO;2, 1998.
1364  Zhang, H., Zhang, M., Jin, J., Fei, K., Ji, D., Wu, C., Zhu, J., He, J., Chai, Z., Xie, J., Dong, X.,
1365      Zhang, D., Bi, X., Cao, H., Chen, H., Chen, K., Chen, X., Gao, X., Hao, H., Jiang, J., Kong,
1366      X., Li, S., Li, Y., Lin, P., Lin, Z., Liu, H., Liu, X., Shi, Y., Song, M., Wang, H., Wang, T.,
1367      Wang, X., Wang, Z., Wei, Y., Wu, B., Xie, Z., Xu, Y., Yu, Y., Yuan, L., Zeng, Q., Zeng, X.,
1368      Zhao, S., Zhou, G., and Zhu, J.: Description and Climate Simulation Performance of CAS-
1369      ESM Version 2, Journal of Advances in Modeling Earth Systems, 12, e2020MS002210,
1370      https://doi.org/10.1029/2020MS002210, 2020a.
1371  Zhang, Z., Barlage, M., Chen, F., Li, Y., Helgason, W., Xu, X., Liu, X., and Li, Z.: Joint
1372      Modeling of Crop and Irrigation in the central United States Using the Noah-MP Land
1373      Surface Model, Journal of Advances in Modeling Earth Systems, 12, e2020MS002159,
1374      https://doi.org/10.1029/2020MS002159, 2020b.
1375  Zhao, G. and Gao, H.: Automatic Correction of Contaminated Images for Assessment of
1376      Reservoir Surface Area Dynamics, Geophysical Research Letters, 45, 6092–6099,
1377      https://doi.org/10.1029/2018GL078343, 2018.
1378  Zhou, T., Leung, L. R., Leng, G., Voisin, N., Li, H.-Y., Craig, A. P., Tesfa, T., and Mao, Y.:
1379      Global Irrigation Characteristics and Effects Simulated by Fully Coupled Land Surface,
1380      River, and Water Management Models in E3SM, Journal of Advances in Modeling Earth
1381      Systems, 12, e2020MS002069, https://doi.org/10.1029/2020MS002069, 2020.
1382